γ spectroscopy of calcium nuclei around doubly magic ^{48}Ca using heavy-ion transfer reactions

D. Montanari,[1,2,*] S. Leoni,[1,2,†] D. Mengoni,[3,4] J. J. Valiente-Dobon,[5] G. Benzoni,[2] N. Blasi,[2] G. Bocchi,[1] P. F. Bortignon,[1,2] S. Bottoni,[1] A. Bracco,[1,2] F. Camera,[1,2] P. Casati,[1] G. Colò,[1,2] A. Corsi,[1,2] F. C. L. Crespi,[1,2] B. Million,[2] R. Nicolini,[1,2] O. Wieland,[2] D. Bazzacco,[6] E. Farnea,[6] G. Germogli,[3] A. Gottardo,[3,5] S. M. Lenzi,[3,6] S. Lunardi,[3,6] R. Menegazzo,[6] G. Montagnoli,[3,6] F. Recchia,[3,6] F. Scarlassara,[3,6] C. Ur,[6] L. Corradi,[5] G. de Angelis,[5] E. Fioretto,[5] D. R. Napoli,[5] R. Orlandi,[5,‡] E. Sahin,[5] A. M. Stefanini,[5] R. P. Singh,[5] A. Gadea,[7] S. Szilner,[8] M. Kmiecik,[9] A. Maj,[9] W. Meczynski,[9] A. Dewald,[10] Th. Pissulla,[10] and G. Pollarolo[11]

[1]*Dipartimento di Fisica, University of Milano, Milano, Italy*
[2]*INFN, Sezione di Milano, Milano, Italy*
[3]*Dipartimento di Fisica, University of Padova, Padova, Italy*
[4]*University of the West of Scotland, Paisley, United Kingdom*
[5]*INFN, Laboratori Nazionali di Legnaro, Padova, Italy*
[6]*INFN, Sezione di Padova, Padova, Italy*
[7]*CSIC-IFIC, Valencia, Spain*
[8]*Ruđer Bošković Institute, Zagreb, Croatia*
[9]*The Niewodniczanski Institute of Nuclear Physics, Polish Academy of Sciences, Krakow, Poland*
[10]*Institut für Kernphysik der Universität zu Köln, Köln, Germany*
[11]*Dipartimento di Fisica Teorica, University of Torino and INFN, Sezione di Torino, Italy*

(Received 9 December 2011; revised manuscript received 2 March 2012; published 2 April 2012)

The γ decays of neutron-rich Ca isotopes around ^{48}Ca were measured at Legnaro National Laboratory with the PRISMA-CLARA setup, using the heavy-ion transfer reactions ^{48}Ca on ^{64}Ni and ^{48}Ca on ^{208}Pb at $\approx$6 MeV/A. The work shows the feasibility to perform full in-beam γ spectroscopy with heavy-ion transfer reactions (in terms of angular distributions, polarizations, and lifetimes analysis), providing a method that can be further exploited in the future with heavy targets and radioactive beams. For the one-neutron transfer channels, ^{49}Ca and ^{47}Ca, shell-model and particle-vibration coupling calculations are used to understand the nature of the states. In particular, in both nuclei evidence is found for particle-vibration coupled states based on the 3^- phonon of ^{48}Ca. In the two-neutron transfer channels, ^{46}Ca and ^{50}Ca, the experimental data are in global agreement with predictions based on full fp shell-model calculations.

DOI: 10.1103/PhysRevC.85.044301 PACS number(s): 25.70.Hi, 21.10.Tg, 23.20.En, 27.40.+z

I. INTRODUCTION

One of the most basic issues in nuclear physics concerns the interplay between single-particle and collective degrees of freedom, which is a manifestation of the many-body nature of the atomic nucleus [1]. Nuclei around shell closures are the best candidates to investigate the single-particle excitation spectrum and the coupling between particles and collective vibrations, providing direct information on the composition of the wave function of the nuclear system. The coupling of a single particle to the vibrational motion is the key process at the origin of anharmonicities of vibrational spectra and a building block of phonon-phonon interactions [1,2]. In particular, these couplings are responsible for the damping of collective excitations (as giant resonances), effective masses [3], and the quenching of spectroscopic factors [4], which quantify the nature and purity of the nuclear states in terms of the occupancy of the single-particle orbits in a nucleus.

For many decades, particle-phonon coupled states have been theoretically described by a phenomenological model, originally developed by Bohr and Mottelson [1], based on a weak-coupling approach and on purely phenomenological inputs. At present, this topic starts to be revised from a more microscopic point of view, using consistently either the Skyrme effective interaction [5] or relativistic mean field models [6].

Experimentally, several indications have been found of discrete states of particle-phonon nature, mostly in medium-heavy nuclei [7–12], but it is still an open question whether such states can be considered a general nuclear property, down to the region of medium-light systems and moving away from the stability valley. In particular, for the majority of near-closed shell nuclei the robustness or softness of core excitations still needs to be discussed to determine whether and to what extent single-nucleon excitations on top of core excitations are very pure or not (i.e., what is the coupling strength between particle states and low-lying core excitations, such as vibrations). Therefore, searches for particle-phonon coupled states, particularly moving away from the stability valley (as, for example, in neutron-rich nuclei) will provide information on the robustness or softness of the nuclear collectivity far from stability, complementing experimental studies aiming at the direct observation of single-particle states, such as single-nucleon transfer and knockout reactions [13,14].

Owing to the difficulty in producing n-rich nuclei by standard fusion-evaporation reactions, no firm spectroscopic information has been available for a long time for several

*Present address: University of Padova, Padova, Italy.
†Corresponding author: silvia.leoni@mi.infn.it
‡Present address: IEM-CSIC, Madrid, Spain.

 ©2012 American Physical Society

neutron-rich systems (even adjacent to the stability valley), resulting in only tentative spin-parity assignments for most of the excited states, as follows from low-energy-resolution particle spectroscopy. A breakthrough in this field came in the last decade, when modern γ arrays made feasible in-beam γ spectroscopy with thick targets and low-energy binary reactions in the grazing regime [15]. It has been clearly demonstrated that deep inelastic collisions between heavy ions are a valuable tool for populating moderately neutron-rich nuclei in different mass regions, making it possible to perform spectroscopic studies of exotic systems. However, the rather short lifetimes of the majority of the states (in the picosecond region) have strongly limited a precise determination of their structure in thick target experiments [15]. These types of experiments have paved the way to even more selective studies with binary heavy-ion reactions, which at present are largely profiting from the combined use of efficient γ arrays and large acceptance magnetic spectrometers [16]. Experimental setups of this type are indeed very powerful because they make possible coincident measurements of particles and γ transitions, therefore allowing a detailed study of both reaction mechanisms and nuclear structure properties of weakly populated reaction products [15,16].

Neutron-rich Ca isotopes are among the most important nuclei not only to follow the variation of nuclear structure with neutron excess (having a closed proton shell) but also to search for particle-phonon coupled states, ^{40}Ca and ^{48}Ca both being doubly magic systems. In this paper we present an in-beam γ-spectroscopy study of ^{47,49}Ca and ^{46,50}Ca, which are populated by one-neutron and two-neutron transfer in the heavy-ion binary reaction ^{48}Ca + ^{64}Ni, at $\approx$6 MeV/nucleon. Making use of the PRISMA-CLARA setup [17], at the INFN National Laboratory of Legnaro (Italy), it has been possible to obtain coincident measurements between the ions detected in the PRISMA spectrometer and their γ decay, measured in the CLARA Ge array. The analysis is based on angular distribution and polarization measurements of the γ radiation, making it possible to firmly establish, for the first time, spin and parities of several excited states in $^{46-50}$Ca isotopes. In addition, lifetime analyses are also performed with a differential plunger technique applied to the ^{48}Ca + ^{208}Pb binary reaction to determine the degree of collectivity of the nuclear system and to understand its nature.

For the one-neutron transfer channels ^{47,49}Ca, the experimental results are compared with full fp shell-model calculations and particle-phonon calculations, providing evidence for different types of coupled states. In particular, high-spin members of the multiplets of states arising by coupling a single particle/hole to the 3^- octupole excitation of ^{48}Ca are observed and interpreted.

In the case of the two-neutron transfer channels, ^{46}Ca and ^{50}Ca, previous tentative spin and parity assignments are confirmed [15] and the lifetimes of all observed states are determined (in many case as an upper limit), resulting in $B(^{E}_{M}\lambda)$ values in global agreement with full fp shell calculations. We note that the experimental investigation of systems two nucleons away from closed shells is very relevant because it allows further testing of the nuclear models also in terms of the strength of the pairing interaction.

The paper is organized as follows. In Sec. II we briefly describe the experimental setup, while in Sec. III we discuss the analysis procedure based on angular distributions and polarization of the γ transitions. The studies of the one-neutron transfer channels, ^{47}Ca and ^{49}Ca, are presented in Sec. IV. Special emphasis is given to the details of the particle/hole-phonon calculations, here revised and extended with respect to the original weak-coupling model of Bohr and Mottelson [1]. The two-neutron transfer channels, ^{46}Ca and ^{50}Ca, are discussed in Sec. V in comparison with full fp shell calculations. Conclusions are given in Sec. VI. The Appendix is devoted to the details of particle/hole-phonon calculations.

II. THE EXPERIMENTS

The work discussed in this paper is based on two experiments performed at Laboratori Nazionali di Legnaro of INFN, using the PRISMA-CLARA setup [17]. Both experiments made use of a ^{48}Ca beam provided by the Tandem-ALPI complex, with an average intensity of $\approx$1 pnA.

In the first experiment (named Ca + Ni) the ^{48}Ca beam, at 282 MeV bombarding energy, impinged on a ^{64}Ni target, 0.98 mg/cm^2 thick, placed at 45° with respect to the beam direction. After $\approx$8 MeV energy loss, the energy available in the middle of the target was about twice the Coulomb barrier. Projectile-like products were selected with the magnetic spectrometer PRISMA placed at the grazing angle for this reaction, that is, $\theta_{\rm lab} = 20°$ (with an angular acceptance of $\pm 6°$). Besides a detailed analysis of the reaction dynamics, reported in Ref. [18], the experiment focused on γ-spectroscopy studies exploiting the capabilities of the experimental setup to measure angular distribution and polarization of γ-ray transitions deexciting the levels of the main reaction products [19].

The second experiment (named Ca + Pb) aimed at the measurements of the nuclear lifetimes in the picosecond range using the differential recoil distance Doppler shift (RDDS) method developed for multinucleon transfer reactions with the PRISMA-CLARA setup [20,21]. The ^{48}Ca beam, at 310 MeV bombarding energy, impinged on a 1.0 mg/cm^2 target of enriched ^{208}Pb (at 45° with respect to the beam direction), evaporated onto a 1.0 mg/cm^2 Ta support (facing the beam). In this case, the energy available for the reaction in the middle of the target, after $\approx$15 MeV energy loss, was about 40% above the Coulomb barrier. After the target, a thick 4 mg/cm^2 $^{\rm nat}$Mg foil was used as an energy degrader of the recoiling ejectiles. In total, five target-to-degrader distances (30, 100, 300, 1400, and 2200 μm) were employed, making use of various metallic rings with a thickness accuracy better than 1.0 μm. The projectile-like products were then selected with the magnetic spectrometer PRISMA placed at the grazing angle $\theta_{\rm lab} = 49°$. We note that, owing to the very different kinematics associated with interactions in the Pb target and in the Ta support (corresponding to a difference of $\approx$8° between grazing angles), only reaction products produced in the Pb target were transported through the PRISMA spectrometer.

The configuration of PRISMA and its detector system have been described in detail in Refs. [22–25], while a schematic view of the setup used in the lifetime experiment can be found in Ref. [20].

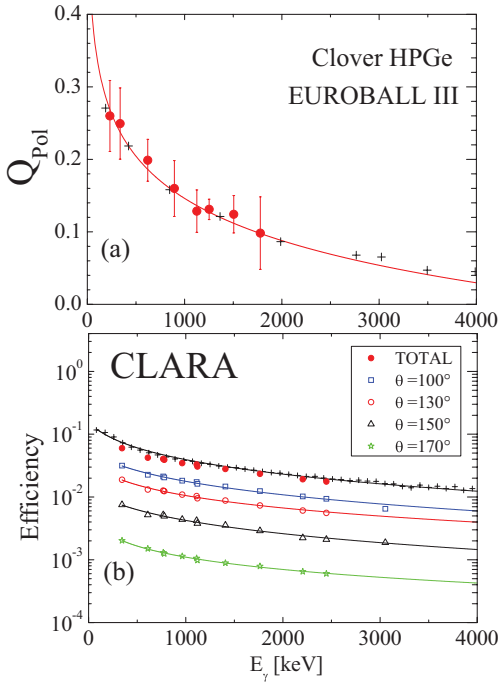

FIG. 1. (Color online) (Bottom) Absolute efficiency of the CLARA Ge array. Crosses refer to simulation calculations for the complete geometry of 25 clover detectors. Solid circles are the experimental measurements for the geometry of 23 detectors, used in the experiments, as obtained with an ^{152}Eu source. The measured efficiencies of the detector rings at $\theta_{CLA} = 100°$, 130°, 150° and of the additional detector at 170° are also shown by open symbols. (Top) The polarization sensitivity Q of the clover detectors [26], as obtained from simulation calculations (crosses) and experimental measurements from known transitions (circles).

In both experiments the CLARA array consisted of 23 high-purity germanium (HPGe) clover-type detectors (out of a total of 25) placed in a 2π configuration close to the target position and opposite to PRISMA [17]. Each clover detector is composed of four crystals mounted in a single cryostat and surrounded by an anti-Compton shield, ensuring a peak-to-total ratio of ∼50%. The total photopeak efficiency of CLARA is of the order of 3% for $E_\gamma = 1.33$ MeV. The clover detectors were arranged in a hemisphere with the Ge crystals placed in three rings at average azimuthal angles $\theta_{CLA} = 100°$, 130°, and 150° with respect to the entrance direction of the spectrometer (defined as $\theta_{CLA} = 0°$). A single additional detector was placed at 170°. In this way, reaction products detected in the spectrometer focal plane have a forward trajectory with respect to the Ge array. Figure 1 shows the absolute efficiency of the CLARA array (bottom panel), as obtained by simulation calculation (crosses) and by measurements with an ^{152}Eu source. The measured efficiency is given for the entire array (circles) and for each ring of detectors, as specified in the legend. The top panel of the figure shows the polarization sensitivity Q of the clover detectors [26], experimentally determined from known transitions and from simulation calculations.

The identification of the reaction products in PRISMA and the Doppler correction of the γ rays emitted by the projectile-like nuclei was completely based upon the reconstruction of the trajectories of the ions in the spectrometer [25], on an event-by-event basis. Both reactions populated several multinucleon transfer channels, with average v/c velocity of ≈10% and ≈2% for projectile- and target-like nuclei, measured at the corresponding grazing angle [i.e., $\theta_{lab}(Ca) = 20°$ and $\theta_{lab}(Ni) = 72°$ in the Ca + Ni reaction and $\theta_{lab}(Ca) = 49°$ and $\theta_{lab}(Pb) = 61°$ in the Ca + Pb case]. These recoil velocity values are confirmed by the Doppler shift analysis of γ rays emitted by the fragments detected in the PRISMA spectrometer. In the Ca + Pb experiment, the recoil velocity of the projectile-like fragments after the degrader was $(v/c)' \approx 9\%$. This value, which is used in the lifetime analysis [20], has been extracted from a typical velocity distribution of the recoiling ions, evaluated for the target-to-degrader distance $d = 300$ μm and it is found to be acceptable for all Ca ions considered in this work. It is also consistent with the energy difference between two shifted lines observed in the γ spectrum at a fixed detector angle. We note that in the lifetime analysis of the Ca + Pb data, only the HPGe detectors placed at 150° were used (with a total photopeak efficiency of ≈1.2%), to avoid uncertainties caused by the Doppler correction. Because of the Doppler broadening the energy resolution in the Ca + Ni experiment was ≈34 keV at 3.8 MeV, which is up to four times larger than in the stopped recoil (thick target) measurements of Ref. [15]. Nevertheless, the centroid values of the γ transitions measured in the present experiments agree within 3 keV with the high-resolution data.

Figure 2 shows the mass distribution of the Ca ions measured in the Ca + Ni experiment, in coincidence with γ rays detected in CLARA. A very good mass resolution is obtained, with a yield of the one-neutron-transfer (^{49}Ca and ^{47}Ca) and two-neutron-transfer (^{50}Ca and ^{46}Ca) channels of the order of 30%–40% and 5%–7% of the population of the inelastic channel ^{48}Ca, respectively. Similar results are obtained for the Ca + Pb experiment. In the present paper we concentrate on spectroscopy studies of Ca isotopes, while for complementary works with PRISMA-CLARA, on K and Ar nuclei, we refer to Refs. [27–29]. Examples of PRISMA-CLARA analysis on heavier systems can be found in Ref. [30].

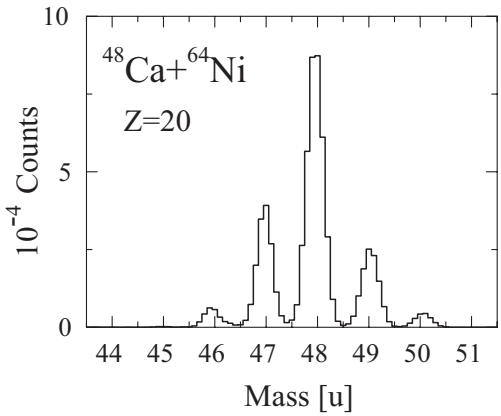

FIG. 2. Mass spectra of the Ca isotopes measured in the ^{48}Ca + ^{64}Ni experiment in coincidence with γ transitions in CLARA.

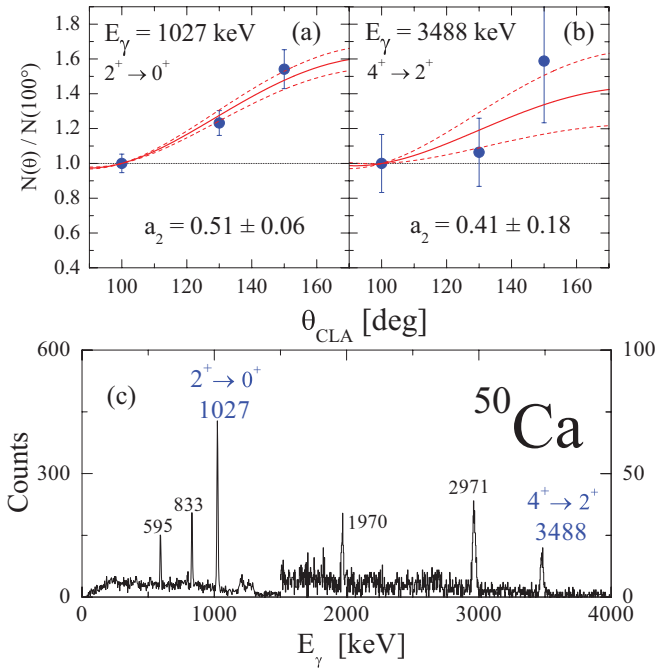

FIG. 3. (Color online) (Bottom) γ spectrum (with 3 keV/channel) measured in coincidence with ^{50}Ca ions detected in PRISMA. Note that above 1500 keV the scale of the y axis is given on the right. Panels (a) and (b): Angular distributions of the $2^+ \rightarrow 0^+$ and $4^+ \rightarrow 2^+$ transitions at 1027 and 3488 keV, respectively. The solid lines are the fit by the angular distribution function $W(\theta) = 1 + a_2 P_2(\cos\theta)$, while the dotted lines give the uncertainty in $W(\theta)$. The extracted a_2 values are given in each panel.

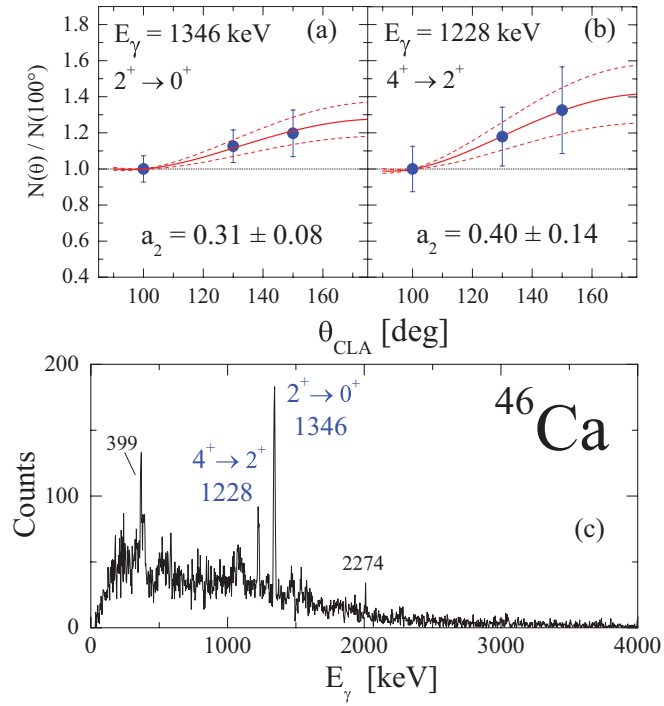

FIG. 4. (Color online) (Bottom) γ spectrum (with 3 keV/channel) measured in coincidence with ^{46}Ca ions detected in PRISMA. Panels (a) and (b): Angular distribution of the $2^+ \rightarrow 0^+$ and $4^+ \rightarrow 2^+$ transitions at 1346 and 1228 keV, respectively. The solid lines are the fit by the angular distribution function $W(\theta) = 1 + a_2 P_2(\cos\theta)$, while the dotted lines give the uncertainty in $W(\theta)$. The extracted a_2 values are given in each panel.

III. ANALYSIS OF THE CLARA DATA

The in-beam spectroscopy study of the $^{46-50}$Ca isotopes has been based on a detailed analysis of angular distributions and polarizations of the γ transitions depopulating the excited states [19]. In addition, the lifetimes of the states in the picosecond range have been determined by the RDDS method [21]. Owing to the limited efficiency of the CLARA array, no γ-γ correlations could be made. This did not affect the analysis, being the level schemes well established by previous works with higher-efficiency arrays [15].

The angular distributions of the strongest γ transitions measured in the Ca + Ni experiment have been studied grouping the Ge detectors in the three rings at $\theta_{CLA} = 100°$, 130°, and 150° (cf. Sec. II). The validity of the analysis has been first demonstrated by studying known $E2$ transitions of ^{50}Ca, ^{46}Ca, and ^{51}Sc, as shown in Fig. 3, 4, and 5. The bottom panel of each figure shows the γ spectrum detected in coincidence with the corresponding ion measured in PRISMA. All strong peaks are transitions with a tentative spin and parity assignments, the only firm cases being the $2^+ \rightarrow 0^+$ and $4^+ \rightarrow 2^+$ decays in ^{50}Ca and ^{46}Ca and the $11/2^- \rightarrow 7/2^-$ transition in ^{51}Sc. The angular distribution analysis of these very intense and clean transitions is also shown in each figure. For each transition, the intensities measured in the three rings have been normalized to the one at 100°, after taking into account the efficiency of each ring (see Fig. 1). The data have been fitted using the angular distribution function $W(\theta) = 1 + a_2 P_2(\cos\theta)$, $P_2(\cos\theta)$ being the Legendre polynomial and a_2 the attenuated angular distribution coefficient (solid line). The dotted lines give the uncertainly in $W(\theta)$ following the error propagation in a_2. Because of the high v/c of the projectile-like products, we have also taken into account the relativistic correction to the angular distribution [31]. The angular distribution coefficient can be

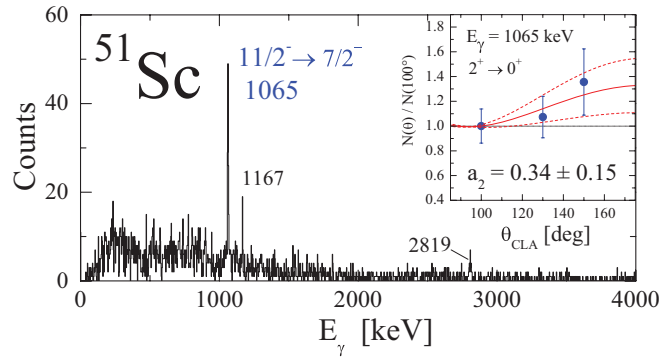

FIG. 5. (Color online) γ spectrum (with 3 keV/channel) measured in coincidence with ^{51}Sc ions detected in PRISMA. The inset of the figure shows the angular distribution of the $11/2^- \rightarrow 7/2^-$ transition at 1065 keV. The solid line is the fit by the angular distribution function $W(\theta) = 1 + a_2 P_2(\cos\theta)$, while the dotted lines give the uncertainty in $W(\theta)$. The extracted a_2 value is given in the inset.

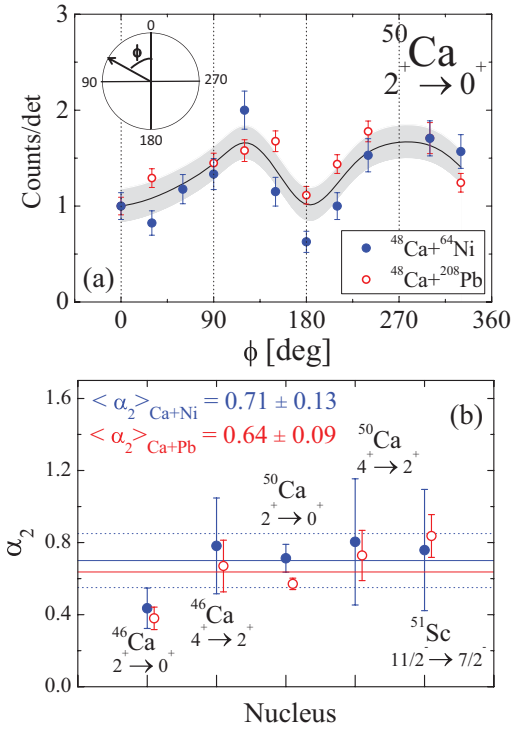

FIG. 6. (Color online) (Bottom) Fraction α_2 of full spin alignment obtained from the experimental angular distributions of known stretched $E2$ transitions, following the decay of ^{46,50}Ca and ^{51}Sc nuclei, populated in the ^{48}Ca + ^{64}Ni and ^{48}Ca + ^{208}Pb reactions (solid and open circles, respectively). The corresponding average values $\alpha_2 = 0.71 \pm 0.13$ and 0.64 ± 0.09 are indicated by solid lines. Dashed lines indicate the uncertainty in the Ca + Ni analysis. (Top) Anisotropy of the $2^+ \rightarrow 0^+$ transition of ^{50}Ca, as a function of the polar angle ϕ at $\theta_{CLA} = 100^\circ$, as measured for both reactions. The average between the two reactions is given by the solid line, while the corresponding uncertainty is indicated by the shaded band. The inset shows the coordinate systems used to define the polar angle ϕ.

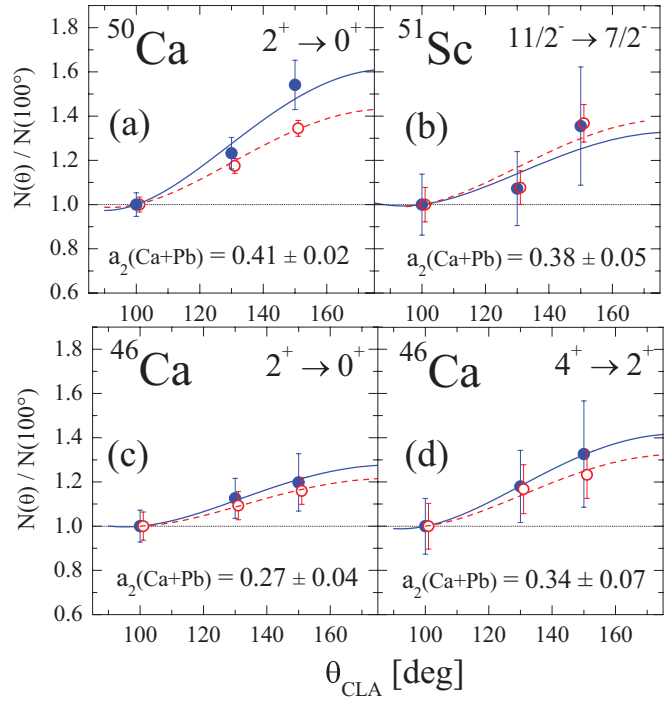

FIG. 7. (Color online) Comparison between the angular distributions of known $E2$ transitions of ^{46,50}Ca and ^{51}Sc nuclei, as follows from the analysis of the Ca + Ni (solid circles) and Ca + Pb data (open circles). Solid and dashed lines are the corresponding fits of the data by the angular distribution function $W(\theta)$, which in the case of Ca + Pb provide the a_2 values given in each panel.

precisely calculated for a given γ decay with fully aligned nuclear spin [32,33], providing a maximum value, a_{2max}, which can be compared with the experiment. It is found that a_{2max} is given by the product A_2B_2, A_2 being the angular distribution coefficient (depending on the multipolarity of the transition) and B_2 the orientation parameter (depending on the orientation mechanism and the spin of the nuclear state). The anisotropy observed in $W(\theta)$ for these $E2$ transitions is consistent with stretched quadrupole decays with a_2 coefficients of the order of 0.3–0.5, as indicated in the figures. This corresponds to a large fraction of spin alignment $\alpha_2 = a_2/a_{2max} = 0.71 \pm 0.13$, as shown by full circles in the bottom panel of Fig. 6. In addition, large oscillations are observed as a function of the polar angle ϕ of the CLARA array. This is shown in the top panel of Fig. 6, in the case of the strong $2^+ \rightarrow 0^+$ transition of ^{50}Ca, measured in the ring at $\theta_{CLA} = 100^\circ$. The anisotropy in ϕ shows maxima at 90° and 270° and minima at 0° and 180°, as expected for a stretched quadrupole decay with the nuclear spin aligned perpendicular to the reaction plane, defined by the PRISMA spectrometer.

The analysis has been also performed on the Ca + Pb data. In this case, the intensities of the transitions of interest have been obtained by summing the intensities of the two components arising from the in-flight emission of ions with two different velocities (before and after the degrader), as later discussed in connection with the lifetime analysis. As shown in Fig. 7, all $E2$ transitions present very similar angular distributions between the two reactions, although a less pronounced anisotropy is observed in the Ca + Pb case. This corresponds to an average fraction of spin alignment $\alpha_2 = 0.64 \pm 0.09$, which is slightly reduced as compared to the Ca + Ni data (cf. Fig. 6). Reduced spin alignments, as compared to standard fusion evaporation reactions, have been reported in the past in heavy-ion transfer reactions at energies around the Coulomb barrier [34,35], similarly to our Ca + Pb case.

The previous analysis clearly shows that a sizable spin alignment, perpendicular to the reaction plane, is a common feature of low-energy binary grazing collisions, involving the exchange of few nucleons. As a consequence, angular distributions and also linear polarization measurements of the γ transitions becomes a powerful tool to firmly establish spin and parity of the nuclear states. In the Ca + Ni reaction, we have tested the possibility of measuring the linear polarization P on the most clean and intense $E2$ transitions, using only the most sensitive clover detectors at 100°. P is defined as the ratio A_{sym}/Q, with $A_{sym} = (N_\perp - N_\parallel)/(N_\perp + N_\parallel)$ the measured asymmetry in the number of photons scattered, in

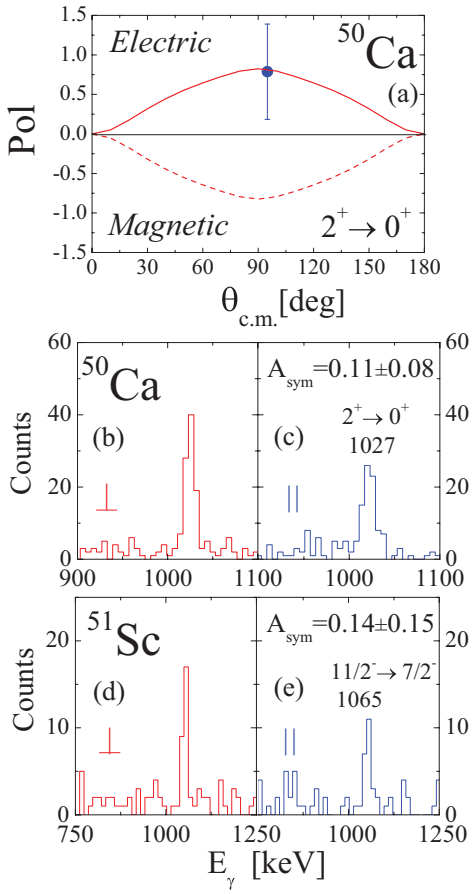

FIG. 8. (Color online) (Bottom and middle) γ spectra of ^{51}Sc and ^{50}Ca in the energy region of the $E2$ decay from the first excited state. Spectra from photons scattered, in the clover crystal, perpendicular ($\perp$) and parallel ($||$) to the emission plane are given on the left and right, respectively. In each case, the asymmetry value A_{sym} is given in the right panel. (Top) comparison between the experimental value of the linear polarization P of the $2^+ \rightarrow 0^+$ transition of ^{50}Ca and the theoretical expectation for a pure electric and magnetic decay, with 70% spin alignment.

the clover crystals, perpendicular ($N_\perp$) and parallel ($N_\parallel$) to the emission plane. Q is the polarimeter sensitivity (shown in Fig. 1). Figure 8 shows the analysis of the $2^+ \rightarrow 0^+$ transition of ^{50}Ca and of the $11/2^- \rightarrow 7/2^-$ transition of ^{51}Sc. In the middle and bottom panels we show spectra corresponding to photons scattering perpendicular ($\perp$) and parallel ($||$), resulting in a clear positive asymmetry A_{sym}, as reported in the legends of panels (c) and (e). This is a strong indication of the electric character of these γ decays, which in the case of the more intense 1027-keV transition of ^{50}Ca gives the linear polarization $P = 0.79 \pm 0.6$, as expected for a stretched $2^+ \rightarrow 0^+$ electric transition with ≈70% spin alignment [cf. Fig. 8(a)].

The angular distribution and linear polarization techniques described above have been used to establish spin and parity of the excited states of $^{46-50}$Ca up to ∼5 MeV of excitation energy. In particular, in the following sections we discuss the one-neutron transfer, ^{49}Ca and ^{47}Ca, and two-neutron transfer channels, ^{46}Ca and ^{50}Ca, for which no firm spectroscopic information is available for the majority of the excited states. To fully interpret the nature of the excited states lifetime measurements have also been performed with the differential plunger technique, and the experimental results (spin, parity, lifetimes) have been compared with shell-model and particle/hole-phonon weak-coupling calculations. A summary of the experimental results is given in Table I.

IV. SPECTROSCOPY OF ONE-NEUTRON TRANSFER CHANNELS

Doubly magic nuclei represent an ideal playground for testing the robustness of nuclear collectivity in different mass regions. This can be done by studying the coupling of a single particle/hole to the vibrational motion of these doubly magic cores. Therefore, adjacent nuclei, just one nucleon away from shell closures, are expected to exhibit energy spectra with both single-particle and coupled-phonon states.

In the case of ^{48}Ca, the 3^- state at 4.507 MeV exhibits a sizable collectivity, with a measured $B(E3)$ of 6.8 ± 1.0 Wu, as follows from electron-scattering experiments [36]. This is also confirmed by Doppler-shift measurements in $(p, p'\gamma)$ reactions, providing the more uncertain value of $10.1^{+6.3}_{-3.3}$ 1 Wu [37]. The rather strong collective character of the 3^- state in ^{48}Ca suggests the existence of multiplets of positive parity states arising by coupling the 3^- phonon with the unpaired $p_{3/2}$ neutron of ^{49}Ca and the $f^{-1}_{7/2}$ neutron hole in ^{47}Ca. Therefore, in the present paper we try to interpret the positive parity states by a particle-phonon model, originally proposed by Bohr and Mottelson [1]. The model is here extended to both particle and hole weak-coupled states, as described in detail in Sec. IV C, to interpret both ^{49}Ca and ^{47}Ca.

The 2^+ state of ^{48}Ca is found instead to exhibit a rather small collectivity, with a $B(E2)$ value of ≈2 Wu, with good agreement between electron-scattering, $(p, p'\gamma)$, and more recent (γ, γ') measurements [36–38]. The yrast 2^+ state of ^{48}Ca has been described as a noncollective 1p1h configuration with a dominating $[f^{-1}_{7/2}, p_{3/2}]$ component [39]. As a consequence, the limited collectivity of the 2^+ state of ^{48}Ca does not support a weak-coupling scheme for the negative parity states of ^{47,49}Ca, which are then better interpreted by shell-model calculations based on either ^{48}Ca- or ^{50}Ca-core states [40]. In the present work, we base our discussion of negative parity states of ^{47,49}Ca on shell-model calculations performed by the code ANTOINE [41,42] in the full fp shell and with the KB3G effective interaction [43]. For the calculation of the transition probabilities standard values of the effective charges for the fp shell have been used ($e_\pi = 1.5e$, $e_\nu = 0.5e$), as established by the lifetime measurement of Ref. [21].

Experimentally, transfer reactions with light ions have provided in past years a wealth of spectroscopic information on a number of excited states of both ^{47}Ca and ^{49}Ca, using the distorted-wave-Born approximation approach [44–49]. In particular, they have firmly established the single-particle nature of the ground states, which is a $p_{3/2}$ neutron state in ^{49}Ca and a $f^{-1}_{7/2}$ neutron hole in ^{47}Ca. In addition, a number of single-particle excited states have been identified, with large spectroscopic factors. Particle spectroscopy has also

TABLE I. Summary of the experimental results obtained for $^{46-50}$Ca nuclei, from the present in-beam γ-spectroscopy work. The a_2 angular distribution coefficients and the $A_{\rm sym}$ asymmetry values are obtained from the Ca + Ni data set, while the lifetimes τ are extracted from the analysis of the Ca + Pb experiment. Tentative spin-parity assignments and multipolarities are given in parentheses. The energy of the levels and the relative decay intensities I_γ (called branching in the text) are taken from Refs. [15,53]. The last column reports, when available, values for the reduced transition probability $B(^M_E\lambda)$ calculated with the shell model (SM) or the particle-vibration coupling model (PVC) using the SkX force (see text for details).

Nucleus	$E_{\rm level}$ (keV)	J_i^π	τ[a] (ps)	E_γ (keV)	I_γ (%)	a_2	$A_{\rm sym}$	γ Mult.	Final level (keV, J_f^π)	$B(^M_E\lambda; J_i \to J_f)$ Exp. [Wu]	Theory [Wu]
^{46}Ca	1346.0	2^+	7.3 ± 1.3	1346	100	0.31 ± 0.08	–	$E2$	1346, 0^+	2.59 ± 0.46	0.83 (SM)
	2574.7	4^+	33.9 ± 7.9	1228	100	0.40 ± 0.14	–	$E2$	1346.0, 2^+	0.88 ± 0.21	0.67 (SM)
	2973.9	6^+	$(15.1 \pm 0.8) \times 10^3$[b]	399	100	–	–	$E2$	2574.7, 2^+	0.55 ± 0.03	0.32 (SM)
^{47}Ca	2013.7	$3/2^-$	6.1 ± 0.3	2013.7	100[c]	0.20 ± 0.04	0.05 ± 0.05	$E2$	0, $7/2^-$	0.40 ± 0.02	0.1 (SM)
	2578.5	$3/2^+$	9.6 ± 1.4	564.8	70.3 ± 18.4[c]	0.37 ± 0.05	–	$E1$	2013.7, $3/2^-$	$(3.0 \pm 0.9) \times 10^{-4}$	–
			–	2578.5	29.7 ± 13.1[c]	–	–	$M2$	0, $7/2^-$	0.9 ± 0.4	1.91[g] (PVC)
	2599.7	$1/2^+$	6.8 ± 0.6	586.0	98.7 ± 2.4[c]	–	–	$E1$	2013.7, $3/2^-$	$(5.4 \pm 0.5) \times 10^{-4}$	–
			–	2599.7	<2[c]	–	–	$E3$	0, $7/2^-$	($\lesssim$55)	2.68 (PVC)
	3999.4	$(11/2^+)$	64 ± 16	437.0	23.3 ± 2.4[d]	–	–	$(E1)$	3562.4, $9/2^-$	$(3.3 \pm 0.9) \times 10^{-5}$	–
			–	65.3	18.6 ± 1.8[d]	–	–	$(M1)$	3933.8, $11/2^+$	0.3 ± 0.1	–
			–	3999.4	58.1 ± 1.7[d]	–	–	$(E3)$	0, $7/2^-$	7.4 ± 1.9	7 (PVC)
^{49}Ca	3357.2	$7/2^-$	3.5 ± 1.2	3357.2	100[d]	0.47 ± 0.07	0.05 ± 0.08	$E2$	0, $3/2^-$	0.05 ± 0.02	0.034 (SM)
	4017.5	$9/2^+$	–	150.9	6.7 ± 0.8[d]	–	–	$(E1)$[c]	3866.6, $7/2^-$	$(1.7 \pm 0.4) \times 10^{-3}$	–
			8.5 ± 2.0	660.3	84 ± 1[d]	0.07 ± 0.05	0.08 ± 0.05	$E1$	3357.2, $7/2^-$	$(2.5 \pm 0.6) \times 10^{-4}$	–
			–	4017.5	9.2 ± 0.8[d]	–	–	$E3$	4017.5, $3/2^-$	7.9 ± 2.0	7 (PVC)
^{50}Ca	1026.8	2^+	96 ± 3[e]	1027	100	0.51 ± 0.06	0.11 ± 0.08	$E2$	0, 0^+	0.68 ± 0.02	0.72 (SM)
	2998	(2^+)	<1.0	1970	100	-0.07 ± 0.18	–	$(M1 + E2)$	1026.8, 2^+	$\geqslant$0.3 (E2)	0.96 (SM,E2)
	3997.1	(3^-)	<1.0	2971	100	-0.34 ± 0.14	–	$(E1)$	1026.8, 2^+	($\geqslant$2.7) 10^{-5}	–
	4515.3	4^+	<1.5	3488	98[f]	0.41 ± 0.18	–	$E2$	1026.8, 2^+	$\geqslant$0.1	0.14 (SM)
	4830.8	(4^-)	<1.0	833	100	0.09 ± 0.09	–	$(M1)$	3997.1, 3^-	$\geqslant$0.05	–
	5110.1	(5^-)	<1.0	595	93.7 ± 6.4[f]	-0.06 ± 0.12	–	$(E1)$	4515.3, 4^+	($\geqslant$3) 10^{-3}	–
^{51}Sc	1065	$11/2^-$	28 ± 7[e]	1065	100	0.34 ± 0.15	0.14 ± 0.15	$E2$	0, $7/2^-$	1.9 ± 0.5	1.5 (SM)

[a]The recoil velocity value used for the lifetime analysis is $(v/c)' = 0.086 \pm 0.003$. See text for details.
[b]From Ref. [65].
[c]From Ref. [57].
[d]From Ref. [15].
[e]From Ref. [21].
[f]From Ref. [53].
[g]Theoretical lower and upper limits for B(M2) are 0.75 (if $g_s^{\rm eff} = 0.4 g_s^{\rm free}$) and 2.62 (if $g_s^{\rm eff} = 0.75 g_s^{\rm free}$). See text for discussion.

indicated the presence of states with very anomalous angular distribution of the scattered particles, leading to questionable spin assignments and largely reduced spectroscopic factors, besides rather large uncertainties in excitation energy, owing to the limited energy resolution of the detected particles. These states were never unambiguously identified even in more recent high-resolution γ-spectroscopy studies [15] (e.g., by measuring the character and multipolarity of the transitions involved). Therefore, a tentative spin and parity assignment has been adopted, so far, mostly based on systematics and comparison with model predictions, leaving open, in particular, the interesting issue of the nature of particle-core coupled states.

In the following paragraphs we present the results from the Ca + Ni and the Ca + Pb PRISMA-CLARA experiments, for both ^{49}Ca and ^{47}Ca, focusing in particular on the states which will then be interpreted in terms of particle-core couplings. We note that binary reactions with heavy ions are particularly suited to populate states based on core phonon excitations, because collective modes are strongly enhanced in the reaction entrance channel, both at low and high excitation energies [50]. However, we do not expect to observe all members of the multiplet of states arising by coupling a particle/hole to a phonon, because the transfer process, at low bombarding energies, mainly favors the population of high-spin stretched configuration [51,52]. This is confirmed by our experimental analysis of ^{49}Ca and ^{47}Ca.

A. Spectroscopy of ^{49}Ca

The case of the one-neutron transfer channel, ^{49}Ca, has been discussed in the Letter of Ref. [19]. We here recall the main points of the experimental analysis and we compare the results with the most recent theoretical calculations for particle-phonon states, discussed in detail in Sec. IV C. Figure 9 shows, in the bottom panel, the γ spectrum of ^{49}Ca measured in the Ca + Ni experiment. Besides the decays from the states at 2.023 and 3.991 MeV, identified as $p_{1/2}$ and $f_{5/2}$ single-particle neutron states by particle spectroscopy studies [44–46] (with spectroscopic factors ∼0.8–0.9), γ transitions of 660, 3357, 3585, and 4017 keV (in the right shoulder of the 3.991-MeV peak) are observed. These transitions deexcite states with a tentative spin-parity assignment [15] and largely reduced fraction of single-particle component (i.e., spectroscopic factors $\leqslant$0.3, as follows from particle spectroscopy studies). The corresponding (partial) level scheme of ^{49}Ca is shown in the right part of Fig. 10, together with the experimental information on the 2^+ and 3^- state of ^{48}Ca (left side), which are relevant for this work. Predictions from shell-model and particle-phonon coupling calculations are also shown in the central part of the figure (see later discussion).

The analysis of the γ spectrum of ^{49}Ca has mainly focused on the strongest 660- and 3357-keV transitions. In particular, the angular distributions of the 660- and 3357-keV γ rays, performed on the Ca + Ni data and shown in Figs. 9(a) and 9(b), provide a_2 parameters equal to 0.07 ± 0.05 and 0.47 ± 0.07, respectively. These values are consistent with dipole and quadrupole transitions, respectively, with a small component of quadrupole decay (∼4%) for the 660-keV

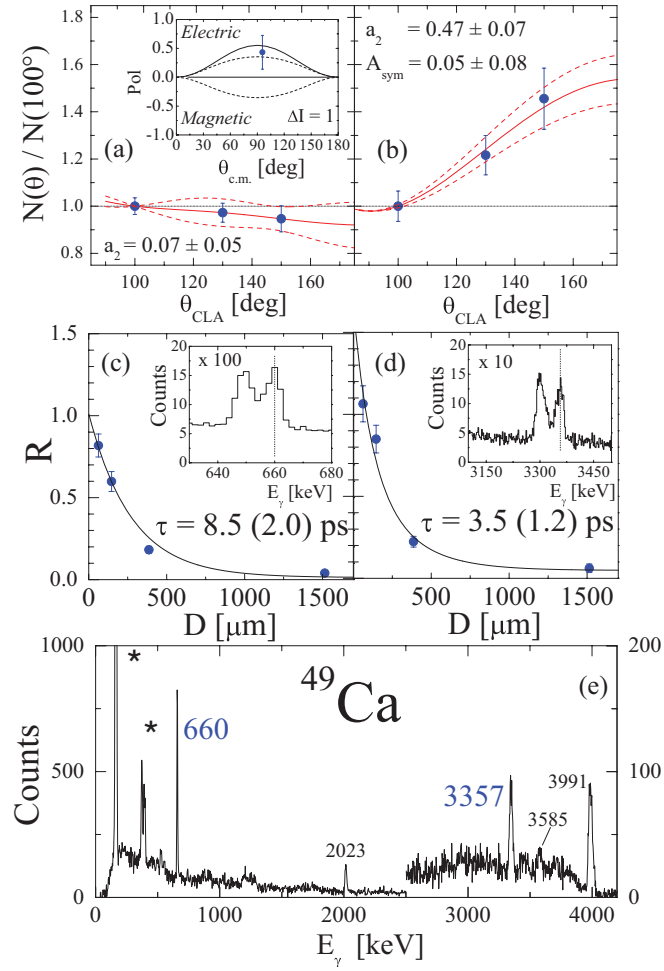

FIG. 9. (Color online) (Bottom) γ spectrum (with 3 keV/channel) measured in coincidence with ^{49}Ca ions in the Ca + Ni experiment. Contaminant lines from the binary partner ^{63}Ni are marked by stars. Note that above 2500 keV the scale of the y axis is given on the right. Top panels (a) and (b): Angular distribution of the 660- and 3357-keV transitions, providing a_2 parameters equal to 0.07 ± 0.05 and 0.47 ± 0.07, respectively. The inset of panel (a) gives the polarization of the 660-keV γ ray, in comparison with prediction for a pure electric or magnetic dipole (dashed lines). The solid line corresponds to the expected values for an electric dipole with a 4% quadrupole component. For the 3357-keV transition the asymmetry value is given. Middle panels (c) and (d): Experimental ratio $R = I_{\text{After}}/I_{660}$ versus the effective target-to-degrader distances, for the 660- and 3357-keV lines, as determined in the Ca + Pb experiment. The inset of each panel shows the two-component structure of each transition, as observed in the γ spectrum obtained by summing the plunger measurements at all distances. The dashed lines indicate the position of the components corresponding to the decay after the degrader (adapted from Ref. [19]).

line. In addition, polarization measurements give the positive asymmetry values $A_{\text{sym}} = 0.08 \pm 0.05$ and 0.05 ± 0.08 for the 660- and 3357-keV γ transitions, respectively, which indicate an electric character in both cases. For the more intense 660-keV line the rather reduced error on the asymmetry value makes it possible to determine the polarization of the γ transition, as shown in the inset of panel (a). The

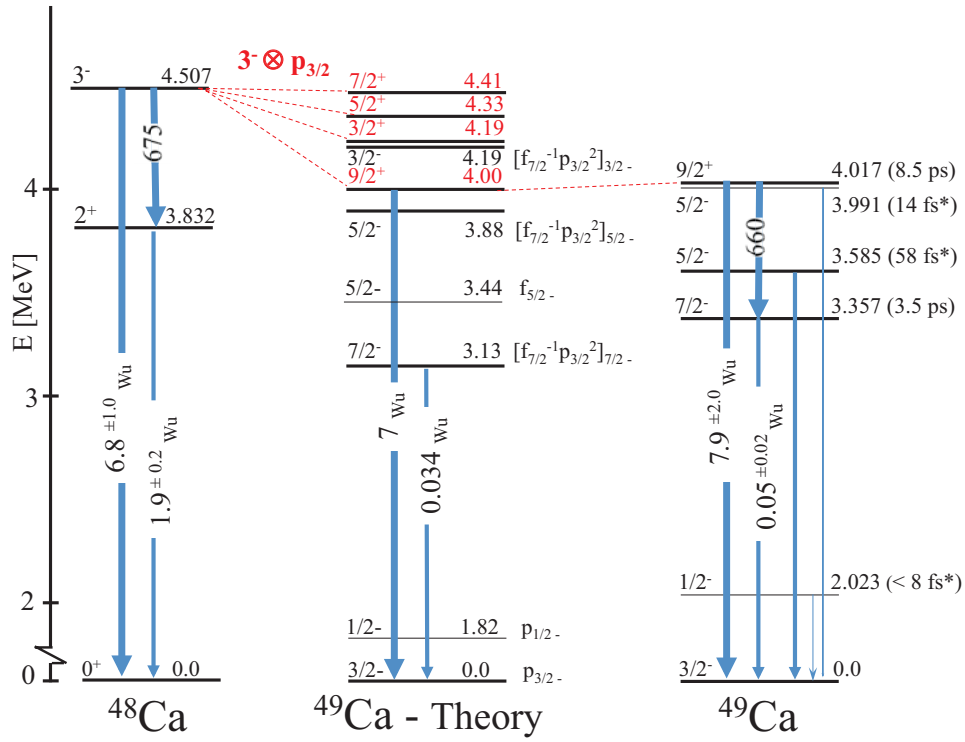

FIG. 10. (Color online) (Right) Decay scheme of ^{49}Ca, as observed in this work. Right labels give the energy of the level (taken from Refs. [15,53]) and its lifetime (in parentheses), as deduced from this work. Stars refer to values taken from Ref. [53]. Thick arrows indicate the decay from particle-phonon coupled states, very thin arrows from states of single particle nature (also indicated by thin lines). (Center) calculated levels of ^{49}Ca. Positive parity states are obtained with the particle-vibration coupling model discussed in Sec. IV C, employing the SkX Skyrme interaction (as discussed in the main text). Negative parity states are calculated by the full fp shell model of Ref. [43], with dominant configurations given on the right side of each level. (Left) experimental 2^+ and 3^- levels of ^{48}Ca. The $B(E\lambda)$ strengths of the relevant γ transitions are reported on the arrows in Weisskopf units (Wu) (from Refs. [36,38] and present work). (Adapted from Ref. [19].)

obtained value $P = 0.43 \pm 0.29$ is consistent with an electric dipole transition with a small admixture ($\approx$4%) of quadrupole component, in agreement with the angular distribution result. Therefore, the present analysis fixes the spin and parity to $9/2^+$ for the 4.017-MeV state and to $7/2^-$ for the 3.357-MeV state.

The nature of the $7/2^-$ and $9/2^+$ states has been investigated through the analysis of the 3357- and 660-keV transitions, measured in the Ca + Pb data by the differential RDDS method. As shown in the insets of panels (c) and (d) of Fig. 9, for both γ transitions two distinct components are observed, depending on whether the γ ray was emitted before or after the degrader. Therefore, the lifetimes of the states of interest are determined by the relative intensities $R = \frac{I_{\rm After}}{I_{660}}$, as a function of the target-to-degrader distances, $I_{\rm After}$ being the peak area after the degrader and I_{660} the total intensity of the 660-keV line. The results of the analysis are shown in panels (c) and (d) of Fig. 9 by solid circles, while the solid lines give the fit of the experimental data by an exponential decay function, which in the case of the 3357-keV level takes also into account, by a two-step decay model [27], the feeding contribution from the 660-keV transition. The lifetimes obtained for the $9/2^+$ and $7/2^-$ states are $\tau = 8.5 \pm 2.0$ and 3.5 ± 1.4 ps, respectively. To get the corresponding $B(E\lambda)$ reduced transition probabilities the decay branching to the ground state has to be taken into account. These are 100% in the case of the $7/2^-$ state and 9.2% in the case of the $9/2^+$ state [15], the latter one giving a partial lifetime of 92 ± 23 ps for the decay via the $E3$ transition of 4017 keV. From these experimental lifetimes we therefore obtain $B(E2) = 0.05 \pm 0.02$ Wu for the 3357-keV transition and $B(E3) = 7.9 \pm 2.0$ Wu for the 4017-keV line, as reported in the right side of Fig. 10 and in Table I. We note that this later value is very close to the $B(E3)$ value of the 3^- state of ^{48}Ca. On the contrary, a much smaller $B(E2)$ value is found for the $7/2^-$ state compared to the corresponding estimate for the 2^+ state of ^{48}Ca. Therefore, we interpret the $9/2^+$ state of ^{49}Ca as a member of the $3^- \otimes p_{3/2}$ multiplet (see IV C), while we will make use of shell-model calculations to interpret the nature of the $7/2^-$ state.

In the case of the $3^- \otimes p_{3/2}$ multiplet, the weak-coupling particle-phonon model provides energies of the multiplet which are shifted with respect to the unperturbed particle plus phonon energy (cf. the later discussion of Fig. 18). As described in Sec. IV C, the calculations have been extended to unambiguously determine the energy of the levels arising by coupling the 3^- phonon with particle states lying in the continuum. Two different parametrizations of the Skyrme force have been tested (SkX [54] and SLy5 [55]), and the results are very similar. In particular, it is found that the energy

of the $9/2^+$ state is 4.00 MeV, which is very close to the experimental value. Moreover, at the lowest perturbative order, the $B(E3)$ value associated with the decay of the member of the multiplet should be equal to the one associated with the phonon deexcitation (the 3^- state in this case), as experimentally obtained for the $9/2^+$ state. We can therefore conclude that there is a strong evidence that the $9/2^+$ state at 4017 keV in ^{49}Ca has a particle-phonon nature. This is expected to be the most favorably populated member of the $3^- \otimes p_{3/2}$ multiplet, because low-energy transfer reactions favor high-spin stretched configuration to maximize the transferred angular momentum [51,52].

Concerning the interpretation of the negative parity states, it is found that the shell-model calculations reproduce rather well both the excitation energy and the $E2$ strength of the $7/2^-$ state, that are, respectively, $E = 3.134$ keV and $B(E2) = 0.034$ Wu, with a dominant configuration (≈80%) of $[f_{7/2}^{-1}\, p_{3/2}^2]$ type. We note that the very different $B(E2)$ values measured for the $7/2^-$ state of ^{49}Ca and the 2^+ state of ^{48}Ca does not support the interpretation of the $7/2^-$ state in terms of a $p_{3/2}$ neutron coupled to the 2^+ state of ^{48}Ca [40]. Furthermore, we point out that 2p1h states with $[f_{7/2}^{-1}\, p_{3/2}^2]$ character (shown in Fig. 10) can, in principle, be generated either by coupling a $p_{3/2}$ particle with the 2^+ state of ^{48}Ca (with dominant configuration $[f_{7/2}^{-1}\, p_{3/2}^2]_2^+$) or by coupling a $f_{7/2}^{-1}$ hole to the 0^+ or 2^+ states of ^{50}Ca, with dominant configuration $[p_{3/2}^2]_{0^+}$ and $[p_{3/2}^2]_{2^+}$, respectively. We are therefore inclined to interpret the $7/2^-$ of ^{49}Ca as a 2p 1h state produced by coupling a $f_{7/2}^{-1}$-neutron hole to the 0^+ core of ^{50}Ca (which is dominated by the paired $[p_{3/2}^2]_0^+$ neutrons). Similar results are obtained by different shell-model calculations [39,56].

B. Spectroscopy of ^{47}Ca

The study of ^{47}Ca (the one-neutron stripping channel) is expected to provide additional information on both single-particle levels and particle-core coupled states around the double-shell closure of ^{48}Ca.

As in the case of ^{49}Ca, angular distribution, polarization, and lifetime measurements performed on the Ca + Ni and Ca + Pb data are here used to shed light on the structural properties of the excited states up to ≈5 MeV of energy. Figure 11 reports, on the right, the partial level scheme of ^{47}Ca, showing all transitions observed in the γ spectrum measured in the Ca + Ni experiment, given in the bottom panel of Fig. 12. The data clearly show the γ decays from the previously known states at 2014 keV ($3/2^-$), 2578 keV ($3/2^+$), and 2599 keV ($1/2^+$), which deexcite emitting γ rays of 2014-, 565-, and 586-keV, besides the direct ground-state decays of 2578 and 2599 keV (seen as a double-peak structure in the γ spectrum). The angular distributions of the first three lines [reported in

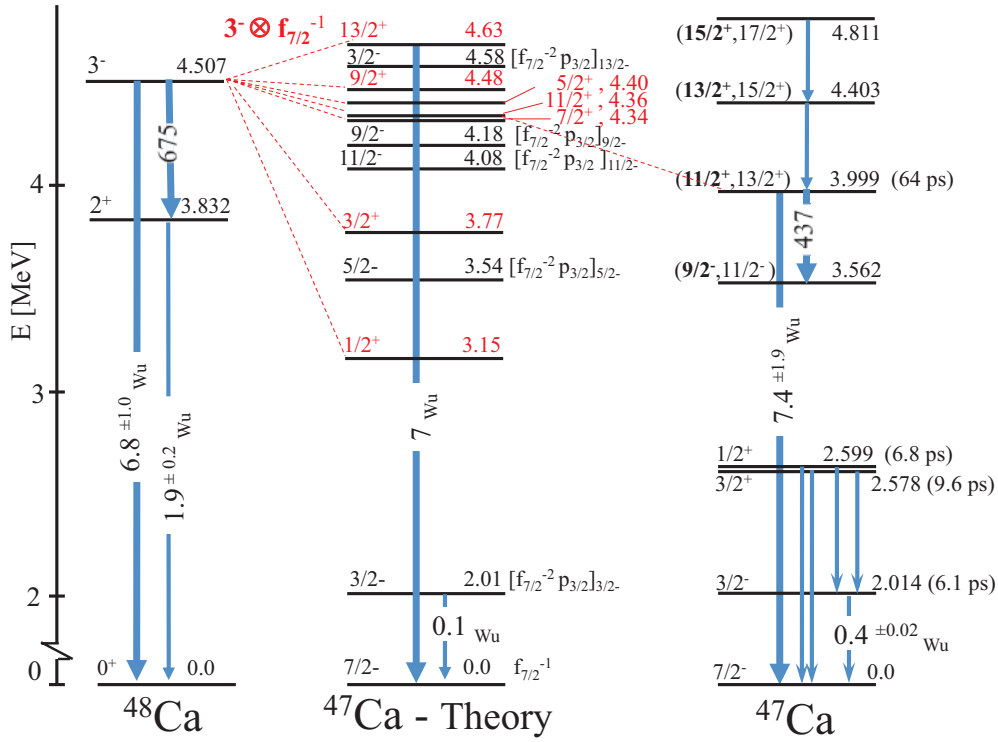

FIG. 11. (Color online) (Right) Decay scheme of ^{47}Ca, as observed in this work. Right labels give the energy of the level (taken from Refs. [15,53]) and its lifetime (in parentheses), as deduced from this work. Thick arrows indicate the decay from states of particle-phonon nature. (Center) Calculated levels of ^{47}Ca. Positive parity states are obtained with the hole-phonon coupling model discussed in Sec. IV C, employing the SkX Skyrme interaction (as discussed in the main text). Negative parity states are calculated by the full fp shell model of Ref. [43], with dominant configurations given on the right side of each level. (Left) Experimental 2^+ and 3^- levels of ^{48}Ca. The $B(E\lambda)$ strengths of the relevant γ transitions are reported on the arrows in Weisskopf units (Wu) (from Refs. [36,38] and present work).

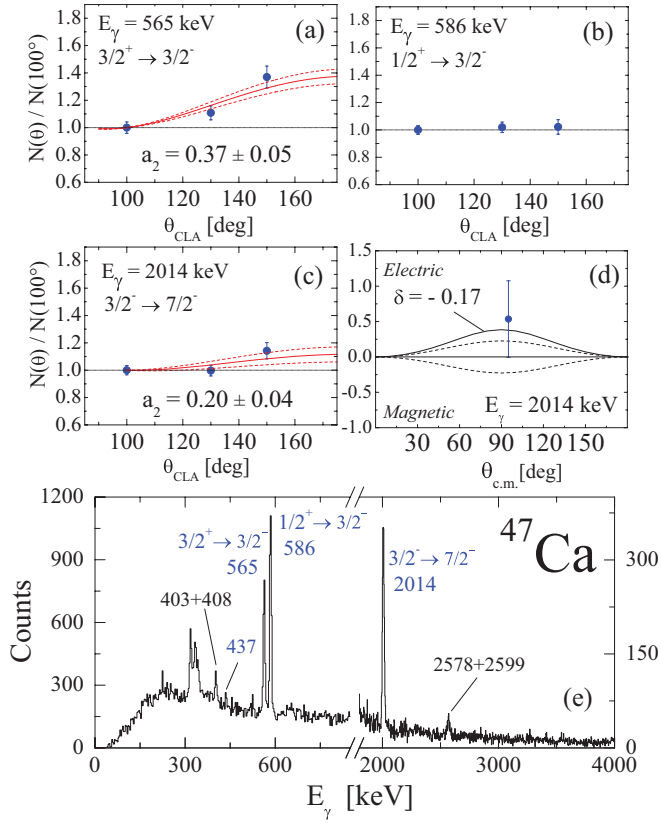

FIG. 12. (Color online) (Bottom) γ spectrum (with 3 keV/channel) measured in the Ca + Ni experiment, in coincidence with ^{47}Ca ions detected in PRISMA. Note that above 1800 keV the scale of the y axis is given on the right. Blue labels indicate transitions studied in details in this work. Panels (a), (b), and (c): Angular distributions of the 565-, 586-, and 2014-keV lines, respectively. The a_2 coefficients are indicated in each panel, except for the 586-keV transition, which is isotropic, being generated by a $1/2^+$ state. Panel (d) shows the polarization analysis of the 2014-keV γ ray. Symbol refers to data, dotted lines to pure electric/magnetic quadrupole transitions. A mixing with octupole component with ≈3% probability ($\delta = -0.17$) is also indicated by a solid line (see text for details).

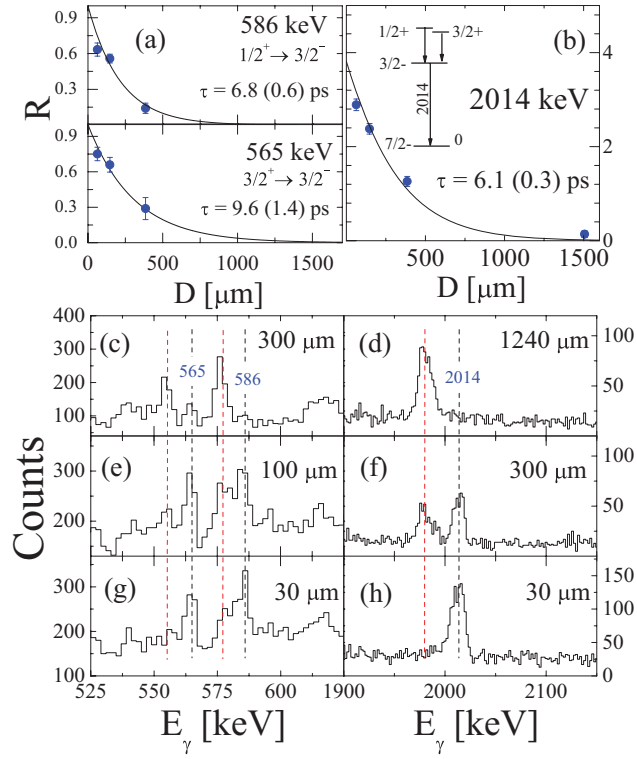

FIG. 13. (Color online) Doppler shift analysis of the 565-, 586-, and 2014-keV lines of ^{47}Ca by the RDDS method. Top panels (a) and (b) show the fit of the intensity ratio R between the high-energy component (corresponding to the decay after the degrader) and the total intensity of the γ-decay line, as observed in the Ca + Pb experiment, at various target-to-degrader distances. In the case of the 2014-keV line, the feeding from the $1/2^+$ and $3/2^+$ states, deexciting by the 586- and 565-keV lines, has been taken into account. Left [right] panels (c), (e), and (g) [(d), (f), and (h)] show the regions of the γ spectrum relevant for the Doppler shift analysis of the 586-, 565-, and 2014-keV lines, respectively. Black (red) lines give the centroid positions of the components decaying after (before) the degrader.

Figs. 12(a)–12(c)] confirm the spin assignments obtained by particle spectroscopy [47–49]. In particular, the 2014-keV line shows an angular distribution which is consistent with the quadrupole decay $3/2^- \rightarrow 7/2^-$ with a small admixture (≈3%) of octupole component, while the electric character of the transition is confirmed by the polarization analysis [see panels (c) and (d)]. The angular distributions of the 565- and 586-keV lines are also in agreement with dipole decays from $3/2^+$ and $1/2^+$ states to a final $3/2^-$ level, as shown in panels (a) and (b). In particular, the angular distribution of the 586-keV line is found to be isotropic, as expected for a decay from a state of spin-$\frac{1}{2}$. The analysis indicates that the 565- and 586-keV lines are stretched $E1$ transitions, while the 2014-keV γ ray has a dominant $E2$ character. We note that the close lying states at 2578 and 2599 keV could not be resolved in particle spectroscopy studies, so that particle data were interpreted assuming a mixture of $1d_{3/2}$ and $2s_{1/2}$ neutron-hole configurations [47–49]. The nature of these states is discussed later in connection with their lifetime analysis and their theoretical interpretation (cf. Sec. IV C).

The results of the Doppler shift measurements for the 565-, 586-, and 2014-keV lines of ^{47}Ca are shown in Fig. 13. For all three transitions a clear double-component structure is observed at various target-to-degrader distances, making it possible to extract a definite value for the lifetime of the nuclear states. From the analysis of the 565- and 586-keV transitions it is found that the lifetimes of the $3/2^+$ and $1/2^+$ levels are 9.6 ± 1.4 and 6.8 ± 0.6 ps, respectively. Moreover, by taking into account their feeding into the $3/2^-$ state by a two-step decay model [schematically illustrated in the inset of Fig. 13(b)], one obtains that the lifetime of the $3/2^-$ level at 2.014 MeV is equal to 6.1 ± 0.3 ps. To estimate the corresponding $B(\frac{E}{M}\lambda)$ reduced transition probabilities one has to consider the branchings of each level, as given in Table I. In particular, the $3/2^+$ is reported to decay with ≈30% branching to the $7/2^-$ ground state; therefore, the partial lifetime is $\tau(2578\ \text{keV}) = 32 \pm 5$ ps, which corresponds to the reduced transition probability $B(M2) = 0.9 \pm 0.4$ Wu.

The $1/2^+$ level is instead reported to decay directly to the ground state with <2% branching [57], therefore giving a partial lifetime $\tau(2599\ \text{keV})$ larger than 500 ps and a $B(E3)$ value smaller than 55 Wu. This unreasonably large upper limit clearly indicates the need for a better estimate of the branching to the ground state for the $1/2^+$ level at 2.599 MeV. We note that in our data the 2599-keV transition is not observed and this supports the extremely low intensity of the decay. For the 565- and 586-keV lines one obtains $B(E1) = (3.0 \pm 0.9) \times 10^{-4}$ and $(5.4 \pm 0.5) \times 10^{-4}$ Wu, which are typical values for $E1$ transitions in this region of mass. Finally, for the 2.014-MeV state, decaying directly with 100% branching to the ground state, one obtains the reduced transition probability $B(E2) = 0.40 \pm 0.02$ Wu.

The γ spectrum of ^{47}Ca measured in the Ca + Ni experiment shows also indications of the 403-, 408-, and 437-keV transitions, previously observed in high-resolution thick-target experiments [15]. These lines correspond to the decay from states at 4.811, 4.403, and 3.999 MeV, with the tentative spin-parity assignments reported in the right side of Fig. 11. The 437-keV line is of particular interest because it deexcites the 3.999-MeV level, which has been suggested as a member of the multiplet arising by coupling the 3^- phonon of ^{48}Ca to the $f_{7/2}^{-1}$ hole of ^{47}Ca. A tentative spin-parity assignment of $11/2^+$ or $13/2^+$ has been assigned to this 3.999-MeV state (with strong preference for $11/2^+$), mostly based on speculation on the energy sequence of the observed states [15]. In the present Ca + Ni experiment, owing to the limited statistics collected for the 437-keV line, no angular distribution analysis could be performed, while an attempt was made to estimate the lifetime of the 3.999-MeV state by the RDDS technique. To focus on the γ decay from the high-excitation-energy region (≈4 MeV) and largely reduce the background in the γ spectrum, a gate on the total kinetic energy loss (TKEL) of the projectile was set. This quantity is measured by the PRISMA spectrometer and it is equal to $-Q$ value of the reaction. As shown in the inset of Fig. 14(a), the Q value for producing the ^{47}Ca nucleus in the ground state is $Q_{gg} = -6$ MeV; therefore, the gate TKEL $= -Q > 11$ MeV is expected to focus on the population of states at ≈4 MeV of excitation energy. The γ spectrum obtained under this condition for the region around the 437-keV transition is shown in Fig. 14 for various target-to-degrader distances. By the Gaussian fit of the peaks shown in panels (b)–(e), the intensities of the high- and low-energy components (corresponding to the decay after and before the degrader, respectively) have been obtained. They are used to determine the ratio R, at different distances, as shown in Fig. 14(a). The lifetime of the 3.999-MeV state extracted from the fit of the ratio R is $\tau = 64 \pm 16$ ps. Taking into account the branching of the state, which is 58% to the ground state, 23% to the 3.562-MeV level, and 18.6% to the 3.934-MeV state (by a 65-keV line, not observed in this data) [15], one obtains the partial lifetime for the direct ground-state decay and for the 437- and 65-keV lines, which are $\tau(3999\ \text{keV}) = 110 \pm 28$ ps, $\tau(437\ \text{keV}) = 275 \pm 75$ ps, and $\tau(65\ \text{keV}) = 344 \pm 92$ ps. This is consistent with the $E1$ character of the 437-keV transition, as suggested by Broda *et al.* [15], with a reduced transition probability $B(E1) = 3.3 \pm 0.9 \times 10^{-5}$ Wu. An $M2$ character would give the unreasonably large value

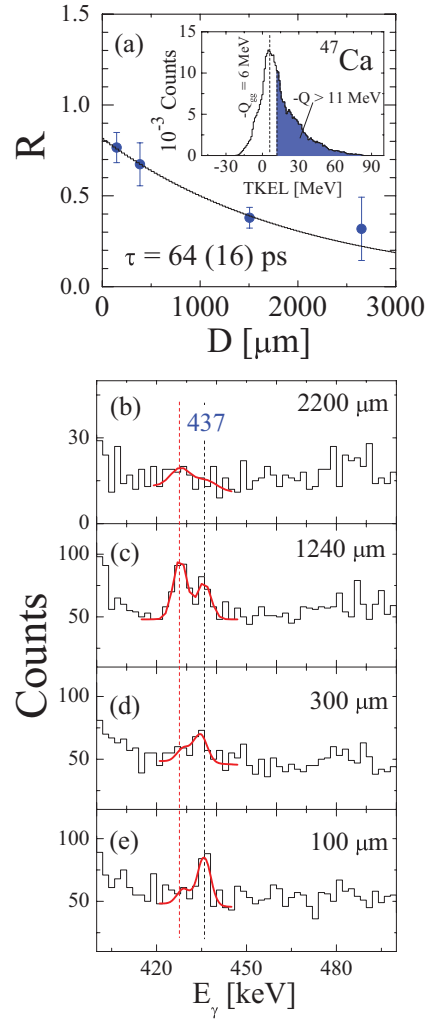

FIG. 14. (Color online) (Bottom panels) γ spectrum of ^{47}Ca at different target-to-degrader distances showing the 437-keV transition (black dotted line) and its Doppler-shifted component at about 430 keV (red dotted line). The spectra have been constructed with the condition TKEL $= -Q > 11$ MeV, as shown in the inset of panel (a). The red lines represent the Gaussian fit for the high- and low-energy components (corresponding to the decay after and before the degrader, respectively), used to determine the ratio R given in panel (a).

$B(M2) \approx 800$ Wu. On the contrary, the 3999-keV line can be interpreted both as an $M2$ or an $E3$, being $B(M2) = 3.04 \pm 0.8 \times 10^{-2}$ Wu and $B(E3) = 7.4 \pm 1.9$ Wu, respectively. Typical values for $M2$ transitions are between 0.03 and 0.1 Wu and for $E3$ transitions between 5 and 20 Wu. We note that the previous $B(E3)$ value is very similar to the 3^- phonon strength of ^{48}Ca, therefore suggesting a possible hole-phonon coupling configuration for the 3.999-MeV state, as discussed in the following and also in Sec. IV C.

Similarly to the case of ^{49}Ca, the interpretation of the excited states of ^{47}Ca has been based on comparison with shell-model calculations, for the negative parity states, while the hole-phonon weak-coupling model has been used for the positive parity states. The results are shown in the central part of Fig. 11. It is found that the shell-model calculations predict the existence of a series of states based on the $[f_{7/2}^{-2}\, p_{3/2}]$

configuration. In particular, the lowest level at 2.01 MeV is the $p_{3/2}$ neutron-particle state arising from promoting a neutron across the $N = 28$ shell, thus producing a $[f_{7/2}^{-2}]_{0^+}$ neutron-hole pair. The predicted $B(E2)$ strength is very small (0.1 Wu) and in reasonable agreement with the experimental value obtained for the 2.014-MeV state.

The positive parity states have instead been calculated considering a weak coupling between the 3^- phonon of ^{48}Ca and the unpaired $f_{7/2}^{-1}$ hole of ^{47}Ca (see Sec. IV C). As shown in the central part of Fig. 11, the model predicts the multiplet of states $J^\pi = 1/2^+$, $3/2^+$, $5/2^+$, $7/2^+$, $9/2^+$, $11/2^+$, and $13/2^+$, with energies shifted with respect to the unperturbed 3^- energy. In particular, all levels are found to be moved down in energy, except for the $13/2^+$ state, which is lifted up by more than 100 keV. Similar results are obtained using both the SkX and SLy5 interactions, as discussed in detail in Sec. IV C. Experimentally, particle spectroscopy studies have shown the existence of many levels around 4–5 MeV of excitation energy, with clear non-single-particle character, rather structureless angular distributions (especially above 5 MeV), and very small spectroscopic factors [47,49]. These states were tentatively interpreted as arising from the $3^- \otimes f_{7/2}^{-1}$ coupling, but no firm spin-parity assignments were established, as well as in a more recent γ-spectroscopy high-resolution experiment [15]. By comparison with the prediction of the weak-coupling model we tend to prefer the $11/2^+$ assignment for the 3.999-MeV state, because it is lower in energy with respect to the 3^- phonon and in agreement (within 400 keV) with the calculated $11/2^+$ level. We note that the present $11/2^+$ assignment has also been favored by Broda *et al.* [15], on the basis of the γ-decay branching argument. As a consequence, the 3.562-MeV level becomes a $9/2^-$ state, having assigned an $E1$ character to the 437-keV transition. This is also in agreement with the particle-spectroscopy work of Ref. [49]. We can therefore conclude that the 3.999-MeV state of ^{47}Ca is another example of particle-phonon coupled state based on the doubly magic core ^{48}Ca.

It is important to note that the $1/2^+$ and $3/2^+$ calculated levels shown in Fig. 11 should correspond to the 2.599- and 2.578-MeV states discussed at the beginning of this section. It is already evident from Fig. 11 that the shift of these two levels with respect to the unperturbed energy is large enough so that the perturbative approach is questionable. We have indeed checked that this approach and the diagonalization of the Hamiltonian including the bare single-nucleon and phonon energies, plus their coupling, give different results and have chosen clearly the results of the diagonalization procedure. The key point to be kept in mind is that perturbation theory is expected to work if the particle-phonon coupling matrix elements are small with respect to the energy differences between unperturbed levels: This is not the case when the energy of the $f_{7/2}^{-1}$ hole plus the 3^- phonon is compared both with the $2s_{1/2}$ and $1d_{3/2}$ hole energies.

We provide the detailed results in Sec. IV C. We summarize here the main points: The wave functions of the two states turn out to be, respectively, $|\frac{1}{2}^+\rangle = 0.837|f_{7/2}^{-1} \otimes 3^-\rangle - 0.547|s_{1/2}^{-1}\rangle$ and $|\frac{3}{2}^+\rangle = 0.765|f_{7/2}^{-1} \otimes 3^-\rangle - 0.644|d_{3/2}^{-1}\rangle$. In both cases, the (hole) spectroscopic factors of these states are neither large nor negligible (≈0.3–0.4). The main decay to the ground state of ^{47}Ca from these states is, respectively, $E3$ and $M2$ (we have explicitly checked that $M2$ by far dominates over $E3$ in the case of the $3/2^+$ decay). In particular, in the case of the $M2$ decay from the $3/2^+$ state, assuming an effective g factor $g_s^{\rm eff} = 0.64 g_s^{\rm free}$, as reported in Ref. [58], one obtains $B(M2) = 1.91$ Wu. However, considering the rather large uncertainty in the quenching of $g_s^{\rm free}$, from 0.4 to 0.75 [59,60], lower and upper limits for this $B(M2)$ values are 0.75 and 2.62, respectively, as reported in Table I.

From the shell-model side, positive parity states involve excitations from the sd shell. We have explored different interactions that allow these type of excitations. None of the calculations are in good agreement with the experimental data. The only interaction that gives the $1/2^+$ and $3/2^+$ states near in energy (less than 100-keV difference) is the $sdfp$ interaction of Ref. [61] in the $s_{1/2}d_{3/2}f_{7/2}p_{3/2}$ model space. The main contribution to the wave function (≈50%) comes from a single-neutron excitation to the fp shell, accompanied by zero, one or two pairs of proton excitations. In this mass region, around $N = 28$, the $1/2^+$ and $3/2^+$ states in P, Cl, and K isotopes are very near in energy and are interpreted as proton single-particle excitations. In fact, as shown in Ref. [62], the effective proton single-particle energies in Ca isotopes cross at $N = 28$.

C. Theoretical model for the particle-vibration coupling in ^{49}Ca and ^{47}Ca

As already stressed, multiplets that appear either in ^{49}Ca or in ^{47}Ca can be associated with states made up with a particle or hole coupled to a vibration of the ^{48}Ca core. Indeed, since the early times of nuclear structure the understanding of the nature of multiplets in odd-nuclei has been one of the main accomplishments of particle-vibration coupling (PVC). As recalled in textbooks [1], the lowest-order corrections to the energy of an unperturbed particle (hole) state plus a core vibration, arise from the perturbative diagrams shown in Fig. 26 (Fig. 27). At the same order, the reduced transition probability $B(E\lambda)$ to the ground state should be the same of the core phonon. The obvious requisite for this picture to make sense is the existence of collective vibrations in the core nucleus. Moreover, we discuss below to what extent the perturbative approach is valid and whether we can go beyond it, at least in the case at hand.

^{48}Ca is known to have a low-lying collective 3^- state. We have tested that theory is able to reproduce the overall properties of this state and then applied the PVC theory. To obtain the results discussed in this section, the following theoretical framework has been adopted. We obtain the single-particle states of the ^{48}Ca core by solving the Hartree-Fock (HF) equations in coordinate space with a Skyrme-type interaction. We use a radial mesh (the step is 0.1 fm), and the sensitivity of the results to the choice of the maximum radius R is discussed below. Unoccupied states are obtained by imposing box boundary conditions at R; that is, the continuum is discretized. We have also calculated the properties of the

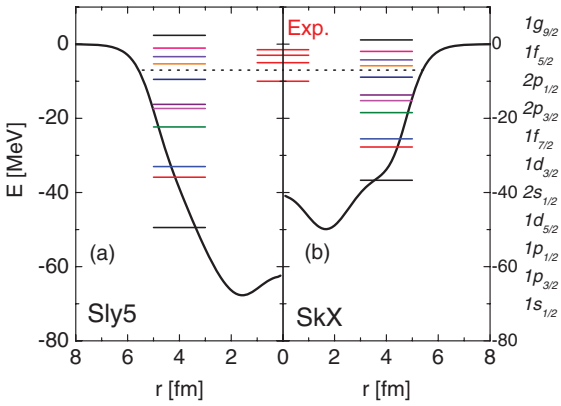

FIG. 15. (Color online) Single-neutron states of ^{48}Ca calculated by means of Hartree-Fock (HF) using the Skyrme forces SLy5 (left) and SkX (right). Solid black lines indicate the central potentials, dotted lines the approximate location of the Fermi surface. States known experimentally are shown in the center of the figure by short red lines.

3^- state in ^{48}Ca by using fully self-consistent RPA in its matrix formulation: This is a well-known framework, and for details on our implementation we refer to Ref. [63] and references therein or to Ref. [64]. We simply remind the reader here that occupied and unoccupied discrete states are used to build a particle-hole (p-h) basis, and the standard RPA matrix equations are written and solved on this basis. The basis dimension (in practice, the upper cutoff on the particle states) is chosen large enough so that the results are stable.

We use for our calculations two different Skyrme sets, namely SkX [54] and SLy5 [55]. The former choice should mimic that of using empirical single-particle states: In fact, the set SkX has been fitted by using the experimentally known single-particle energies in several nuclei, including ^{48}Ca, and has an effective mass that is close to 1. The latter choice corresponds to taking one of the standard and most reliable Skyrme sets. In the case of the calculation of the 3^- we compare also with other existing sets.

The results for the single-particle states are displayed in Fig. 15. The difference in the effective mass is clearly reflected in the different level spacing: This figure makes it clear that we wish to try two forces with quite different single-particle properties. The main properties of the low-lying 3^- state are summarized in Fig. 16. The top (bottom) panel displays the energy (reduced transition probability) obtained by means of RPA. It can be seen that SLy5 reproduces the experimental values quite well. The most important fact to notice is that the experimental value corresponds to 6500 e^2 fm^6, or to 6.8 Wu [36]. Indeed, from the RPA calculation one obtains a state that is not pure single particle. In Table II we show the composition of the 3^- wave function, as obtained using the sets SLy5, LNS, and SkX, which better reproduce the energy and strength of the state. It is found that the state does not have a pure single-particle nature because at least three components do contribute by more than 1%. This vibrational picture is also supported by the simple shape of the transition densities: As one can see from Fig. 17, the

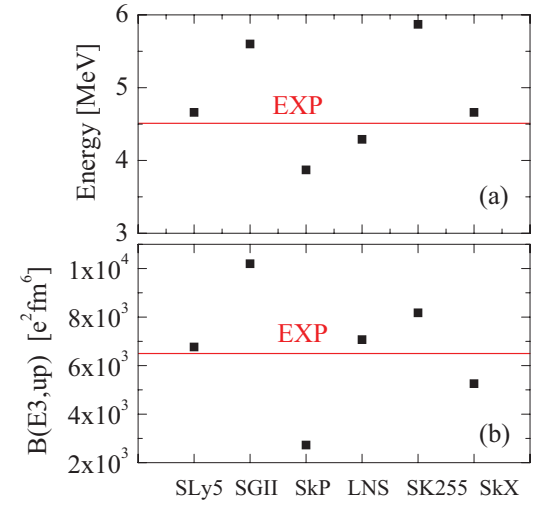

FIG. 16. (Color online) Energy (top) and $B(E3,\text{up})$ (bottom) of the 3^- state of ^{48}Ca, as obtained from RPA calculations using different Skyrme forces. The horizontal lines correspond to the experimental values.

neutron and proton transition densities display only zero or one node.

We discuss then the framework for the PVC calculations. The analytic expressions for the diagrams shown in Figs. 26 and 27 are provided in the Appendix. To evaluate them, the single-particle energies ϵ and RPA energies $\hbar\omega$ are needed. In addition, one must input the PVC matrix element $h(j_2, j_1\lambda)$ (coupling the fermionic state j_2 to the fermion-boson pair made up with j_2 and λ). These are defined as in [1]. It would be, in principle, possible to calculate this matrix element consistently with the Skyrme force used for HF and RPA. Such calculations have been carried out, for example, in Ref. [5], but they turn out to be computationally very demanding. Therefore, we have adopted here the Bohr-Mottelson form for the matrix element h, namely,

$$h(j_2, j_1\lambda) = \frac{(-1)^{j_1+j_2}}{2j_2+1}\sqrt{\frac{\hbar\omega}{2C}}\int dr\, u_{j_2}u_{j_1}k_\lambda(r)\langle j_1\|Y_\lambda\|j_2\rangle. \quad (1)$$

In this formula, the factor $\sqrt{\hbar\omega/2C}$ is related to the reduced transition probability of the phonon state in the standard way [1], u are the radial (HF) wave functions, and k_λ is taken as the derivative of the HF mean field. The radial integrals that appear in this equation are close to the standard value of $\approx$50 MeV

TABLE II. Values of the squared RPA amplitudes associated with the p-h components of the wave function of 3^- in ^{48}Ca, obtained by means of RPA calculations using different Skyrme forces. We display values which are larger than 0.01 or 1% (associated with amplitudes larger than 0.1).

p-h component	SLy5	LNS	SkX
$\pi 1d_{3/2} \to 1f_{7/2}$	0.83	0.66	0.18
$\pi 2s_{1/2} \to 1f_{7/2}$	0.13	0.31	0.78
$\nu 1f_{7/2} \to 1g_{9/2}$	0.01	0.02	0.03

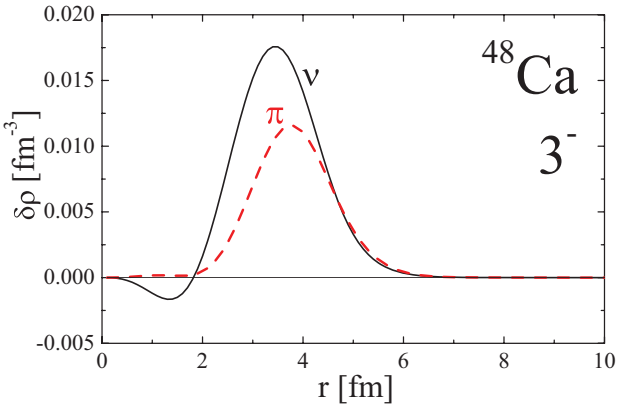

FIG. 17. (Color online) Transition densities of the 3^- state of ^{48}Ca, for neutrons and protons, obtained by RPA calculations with the SLy5 interaction.

for states around the Fermi energy, but they differ for deeply lying states or for weakly bound or quasibound states.

In the present work we have dealt with the problem of whether the calculation of PVC made in a finite box, which allows continuum discretization, is stable. We have performed calculations of the energy shifts of all the members of multiplets in ^{49}Ca and ^{47}Ca by varying the box size R between 15 and 25 fm. If we look at the expressions of the diagrams provided in the Appendix, we can understand the following argument that supports our numerical finding, namely that the energy shifts are stable with respect to variations of the box size. The energy denominators of the perturbative diagrams tend to decrease with the increase of the box size because of the decrease of the energy of the states in the discretized continuum.

At the same time, the quantities h^2 tend also to decrease with the increase of the box because of the spill out of the radial wave functions and their reduced overlap with the form factor $k_\lambda(r)$. As a net result our energy shifts are stable, as shown in Figs. 18 and 19. The energies of the members of the multiplet,

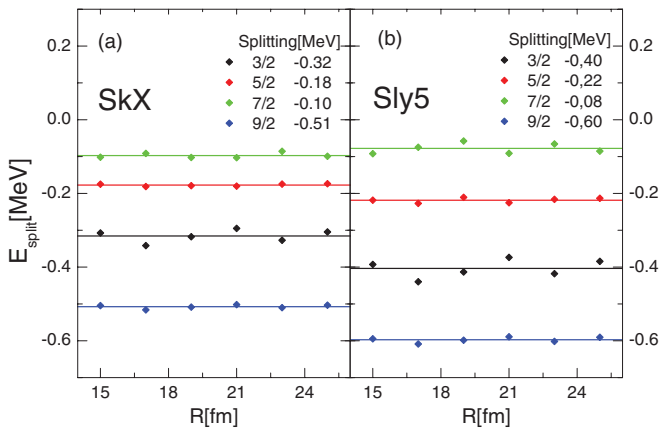

FIG. 18. (Color online) Energy splitting of the $3 \otimes p_{3/2}$ multiplet of ^{49}Ca for different values of the box dimension R adopted in the Hartree-Fock calculation with a SkX (left) and Sly5 (right) interaction. The average energy splitting for each multiplet member is given in the legend.

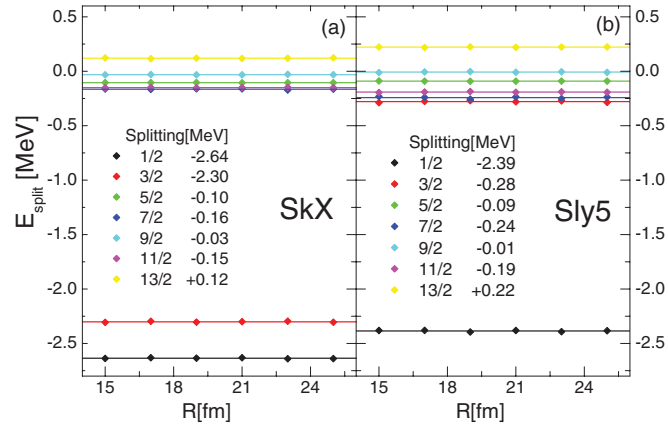

FIG. 19. (Color online) Energy splitting of the $3 \otimes f_{7/2}^{-1}$ multiplet of ^{47}Ca for different values of the box dimension R adopted in the Hartree-Fock calculation with the SkX (left) and SLy5 (right) interactions. The average energy splitting for each multiplet member is given in the legend.

that is, the unperturbed energies plus these energy shifts, have been used in the above figures and compared with experiment. As already mentioned, within this perturbative approach the $B(E3)$ values for the decay to the ground state are equal to the $B(E3)$ of the phonon in the core nucleus ^{48}Ca.

Only in the case of two states in ^{47}Ca, the $1/2^+$ and $3/2^+$ that have been already discussed above, the perturbative approach is not satisfactory. It turns out that the coupling of these two states, respectively, with the pure single-particle states $2s_{1/2}$ and $1d_{3/2}$ (diagram associated with V_a in Fig. 27) is too strong to be treated perturbatively. Consequently, for these two cases, we have diagonalized the two-by-two matrix including the unperturbed energies of the hole and hole plus phonon states, plus their coupling.

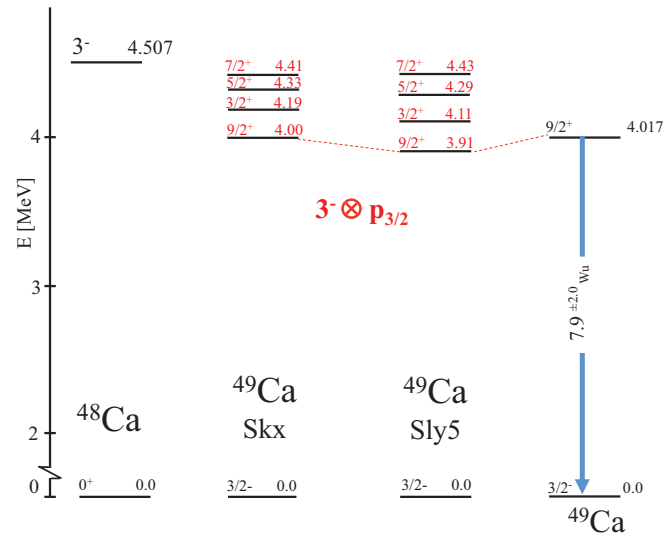

FIG. 20. (Color online) Decay scheme of ^{49}Ca from particle-phonon model calculations using the SkX and Sly5 forces. Experimental data for ^{48}Ca and ^{49}Ca are shown on the left and right side, respectively.

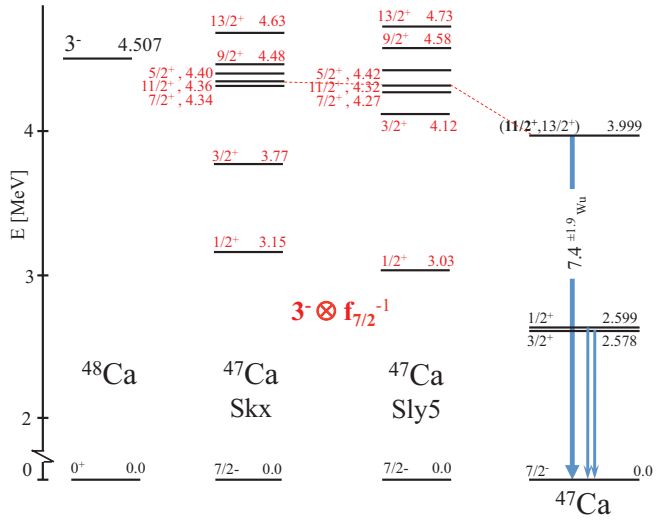

FIG. 21. (Color online) Decay scheme of ^{47}Ca from hole-phonon mode calculations using the SkX and Sly5 forces. Experimental data for ^{48}Ca and ^{47}Ca are shown on the left and right side, respectively.

To analyze the sensitivity of the results to the choice of the Skyrme parameter set, we have performed calculations with the two sets SkX and SLy5. The results are compared in Fig. 20 for ^{49}Ca and in Fig. 21 for ^{47}Ca. For ^{49}Ca and for most of the levels in ^{47}Ca, the two sets predict quite similar results. As one could expect, differences arise when the weak-coupling approximation breaks down (i.e., in the case of $1/2^+$ and $3/2^+$ in ^{47}Ca). We have discussed in Sec. IV B the results associated with the interaction SkX, because its single-particle levels are closer to experiment. The wave functions of the two states $1/2^+$ and $3/2^+$ have been written above as $|\frac{1}{2}^+\rangle = 0.837|f_{7/2}^{-1}\otimes 3^-\rangle - 0.547|s_{1/2}^{-1}\rangle$, and $|\frac{3}{2}^+\rangle = 0.765|f_{7/2}^{-1}\otimes 3^-\rangle - 0.644|d_{3/2}^{-1}\rangle$. For comparison, we report here the same wave functions in the case of the interaction SLy5, which read $|\frac{1}{2}^+\rangle = 0.786|f_{7/2}^{-1}\otimes 3^-\rangle - 0.214|s_{1/2}^{-1}\rangle$ and $|\frac{3}{2}^+\rangle = 0.914|f_{7/2}^{-1}\otimes 3^-\rangle - 0.086|d_{3/2}^{-1}\rangle$. In the case of SLy5, the mixing of the members of the multiplet with pure single-nucleon components is smaller, in keeping with the larger energy differences (or, in other words, with the smaller effective mass). Accordingly, the $E3$ transition probability of the $1/2^+$, which is associated with the phonon component, is larger in the case of SLy5 (3.37 W.u.) than in the case of SkX. On the contrary, the $M2$ transition probability of the $3/2^+$ state, that scales with the square of the pure single-particle amplitude, is significantly smaller in the SLy5 case (0.03 W.u.) than in the case of SkX.

V. SPECTROSCOPY OF TWO-NEUTRON TRANSFER CHANNELS

Two-nucleon transfer channels represent a test bench for both reaction dynamics and nuclear structure models, in particular because the pairing interaction plays a crucial role in this case. In the present work we concentrate on two-neutron stripping and pickup channels, that is, on ^{46}Ca and ^{50}Ca,

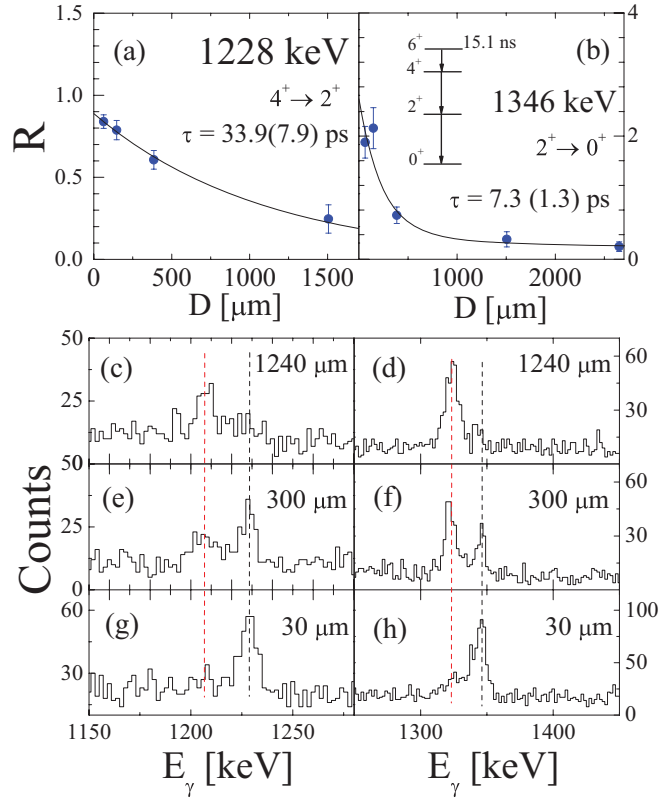

FIG. 22. (Color online) (Bottom) γ spectra of ^{46}Ca, at different target-to-degrader distances, showing the $4^+ \rightarrow 2^+$ transition at 1228 keV (left) and the $2^+ \rightarrow 0^+$ decay at 1346 keV (right), together with their Doppler shifted components. (Top) Interpolations of the ratio R, providing the lifetime τ of the 4^+ and 2^+ states.

populated in the ^{48}Ca + ^{64}Ni and ^{48}Ca + ^{208}Pb reactions. The experimental study, mostly based on angular distribution and lifetime analysis, makes it possible to determine, more precisely, spin and parity of the excited states and to establish their nature. Positive parity states will then be interpreted in terms of shell-model calculations based on the ANTOINE code [41,42], using the same framework adopted in the case of the one-neutron transfer channels discussed in Sec. IV, that is, full fp shell, KB3G effective interaction, and standard effective charges ($e_\pi = 1.5e$, $e_\pi = 0.5e$).

A. Spectroscopy of ^{46}Ca

Although a stable nucleus, ^{46}Ca is poorly known, mostly owing to its extremely small abundance (only 0.004%), which makes it very difficult to perform, for example, Coulomb excitation experiments [66]. As discussed in the paper of Speidel *et al.* [66], Coulomb excitation and g factor measurements of the first 2^+ state of ^{46}Ca, at 1346 keV, tend to exclude substantial excitations of protons and neutrons from the sd shell below $Z = 20$. This strongly differs from similar measurements performed on the 2^+ state of ^{42}Ca and ^{44}Ca, clearly indicating the need for a large admixture of particle-hole configurations from ^{40}Ca core excitations to explain consistently both the measured g factors and the $B(E2)$

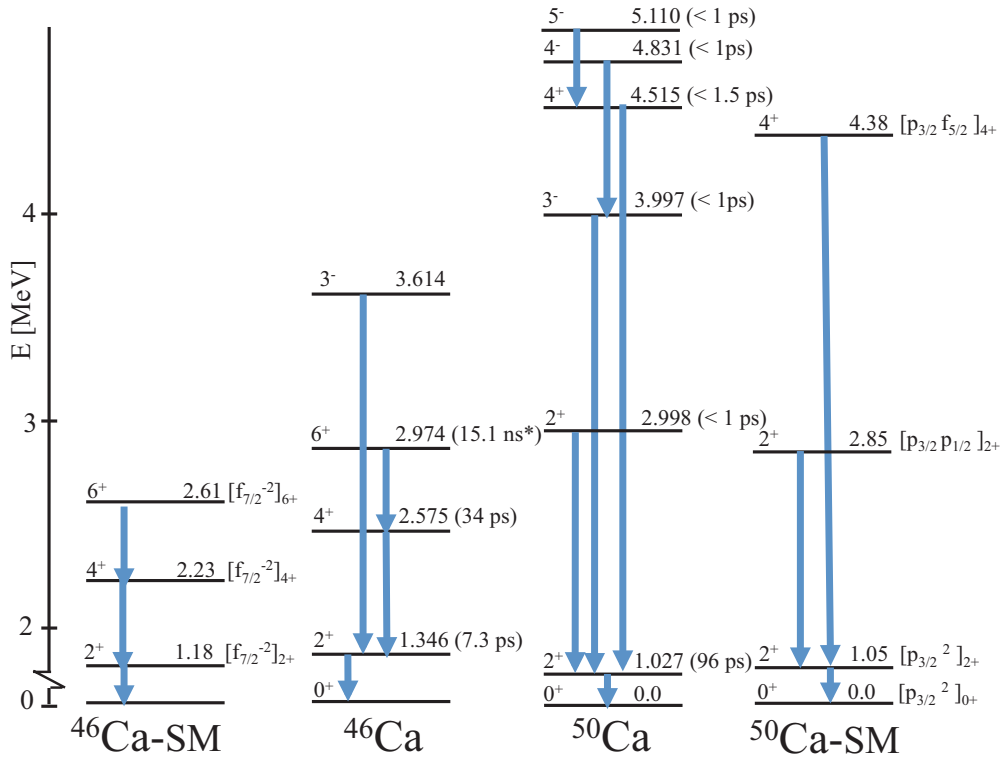

FIG. 23. (Color online) Decay scheme of ^{46}Ca (left) and ^{50}Ca (right), as observed in this work, in comparison with shell-model calculations performed by the ANTOINE code of Ref. [43], with full fp shell and KB3G force. Dominant configurations are given on the right side of each level. Experimental level energies (right labels) are taken from Refs. [15,53]. Experimental lifetimes are obtained from this work, except for the 6^+ state of ^{46}Ca (marked by *), which is taken from Ref. [65]. Comparisons between data and theory in terms of $B(^M_E\lambda)$ values are given in Table I.

values. As an alternative technique, multinucleon transfer reactions provide a valuable way to populate excited states up to rather high spins, making it possible to perform a more stringent comparison between experimental data and shell-model predictions over a wider range of excited states.

The γ spectrum measured in the Ca + Ni experiment in coincidence with ^{46}Ca ions detected in the PRISMA spectrometer has already been shown in Fig. 4, together with the angular distributions of the 1346- and 1228-keV lines, clearly confirming the stretched $E2$ character of the $2^+ \rightarrow 0^+$ and $4^+ \rightarrow 2^+$ transitions. In addition, lines at 399 and 2274 keV are visible in the γ spectrum, corresponding to the previously known $6^+ \rightarrow 4^+$ and $3^- \rightarrow 2^+$ decays. The lifetimes of the 2^+ and 4^+ states have been determined by the RDDS method applied to the Ca + Pb data, and the results of the analysis are shown in Fig. 22. As reported in Ref. [65], the 6^+ state, feeding the 4^+ state, has a lifetime of the order of 15 ns. Therefore, we have first evaluated the lifetime of the 4^+ state, assuming a feeding from a state with a lifetime 10^2–10^3 times longer than for the state of interest. As shown in the top panel (a), the fit of the ratio R gives the lifetime $\tau = 33.9 \pm 7.9$ ps, which corresponds to the reduced transition probability $B(E2, 4^+ \rightarrow 2^+) = 0.88 \pm 0.21$ Wu. In the case of the 2^+ state, the lifetime has been evaluated making use of a two-steps decay model, taking into account the lifetime of the 4^+ state (determined above) and the relative population of the two states. The analysis gives the value $\tau = 7.3 \pm 1.3$ ps, which agrees well, within the error bar, with the most recent Coulex measurement, reported in Ref. [66]. The corresponding reduced transition probability is $B(E2, 2^+ \rightarrow 0^+) = 2.59 \pm 0.46$ Wu. Figure 23 shows, on the left, the partial decay scheme of ^{46}Ca, as observed in this work, in comparison with shell-model calculation for positive parity states. As also reported in Table I, the agreement is rather satisfactory, also in terms of $B(E2)$ strength, which in the worst case (the $2^+ \rightarrow 0^+$ decay) under estimates the experimental value by approximately a factor of 3. This indicates that the first excited states of ^{46}Ca can be rather well interpreted by shell-model calculations including the full fp shell, without invoking any core excitation. In fact, the 2^+, 4^+, and 6^+ states are found to originate by a $f_{7/2}^{-2}$ neutron-hole pair, as shown on the left-hand side of Fig. 23. This agrees with the results reported in Ref. [66] which, on the basis of g factor measurements of Ca nuclei, strongly indicated a dominant contribution from valence neutron of the fp shell.

B. Spectroscopy of ^{50}Ca

The neutron-rich nucleus ^{50}Ca is expected to have a rather simple structure, involving mainly two neutrons in the $p_{3/2}$ orbital moving around the doubly magic nucleus ^{48}Ca. The extended γ-spectroscopy work reported in Ref. [15], based on binary reactions with thick targets, has made it possible to

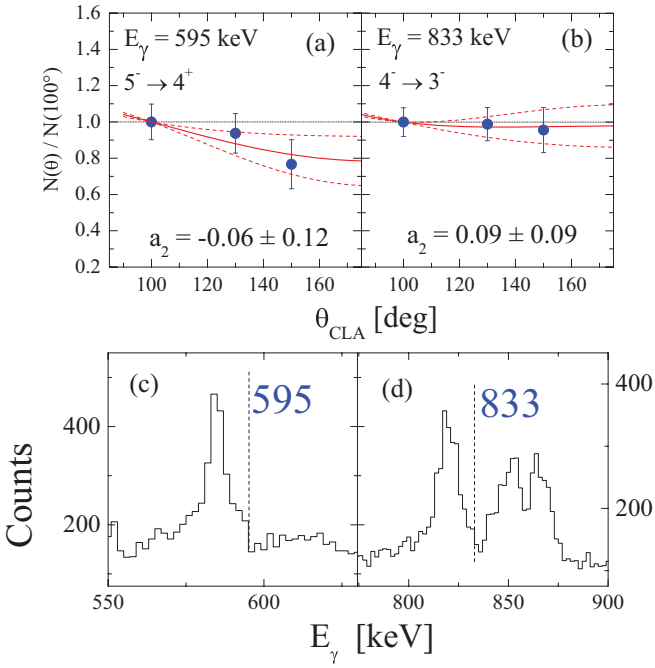

FIG. 24. (Color online) ^{50}Ca. Panels (a) and (b): Angular distributions of the 595- and 833-keV lines, as obtained from the Ca + Ni data. The a_2 coefficients reported in the panels are compatible with dipole transitions between the indicated levels, with small admixture of quadrupole decays (≈1.5% and 6%, respectively). Panels (c) and (d): γ spectrum of ^{50}Ca summed over all target-to-degrader distances used in the Ca + Pb plunger experiment. The energy regions relevant for the Doppler shift analysis of the 595- and 833-keV lines are displayed, with dashed lines indicating the expected position for the component corresponding to the decay after the degrader.

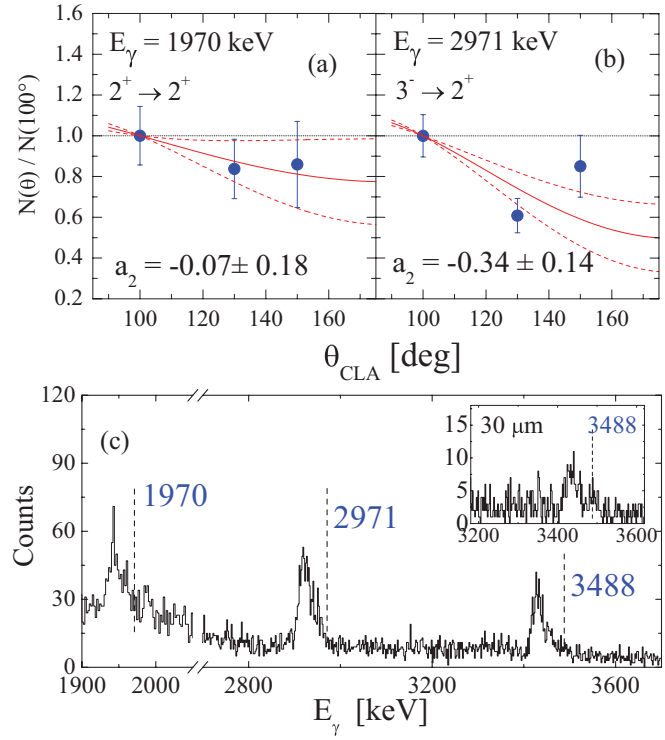

FIG. 25. (Color online) ^{50}Ca. Panels (a) and (b): Angular distributions of the 1970- and 2971-keV lines, as obtained from the Ca + Ni data. The a_2 coefficients reported in the panels are compatible with dipole transitions between the indicated levels, with admixture of quadrupole decays of the order of ≈16% and <1%, respectively. Panel (c): γ spectrum of ^{50}Ca summed over all target-to-degrader distances used in the Ca + Pb plunger experiment. The energy region relevant for the Doppler shift analysis of transitions at 1970, 2971, and 3488 keV is displayed, with dashed lines indicating the positions of the high-energy components corresponding to the decay after the degrader. The inset shows the 3488-keV line measured at the shortest distance of 30 μm, with indication of a very weak high-energy component.

establish the excitation spectrum up to ≈7 MeV, although no firm experimental information is given for spin and parity of the majority of the states. In the present work we measure, with some uncertainty, the angular distributions of the strongest γ transitions of ^{50}Ca and we provide upper limits for the lifetimes of the corresponding excited states.

The γ spectrum of ^{50}Ca measured in the Ca + Ni experiment has already been shown in Fig. 3, together with the angular distributions of the known $2^+ \rightarrow 0^+$ and $4^+ \rightarrow 2^+$ transitions at 1027 and 3488 keV, respectively. Panels (a) and (b) of Fig. 24 show the anisotropies of the low-energy transitions at 595 and 833 keV, which are characterized by very small a_2 coefficients, compatible with $5^- \rightarrow 4^+$ and $4^- \rightarrow 3^-$ dipole transitions, with a small admixture (≈1.5% and 6%, respectively) of quadrupole decays. The anisotropies of the higher-energy transitions at 1970 and 2971 keV, shown in panels (a) and (b) of Fig. 25, are also consistent with dipole transitions between the $2^+ \rightarrow 2^+$ and $3^- \rightarrow 2^+$ states, with <1% contaminant from quadrupole decay in the case of the 2971-keV line. On the contrary, for the 1970-keV transition a larger admixture of quadrupole decay is found (≈16%). We note that for all four analyzed transitions, the rather large error bars and the few angles available for the angular distribution analysis do not allow to obtain more accurate results. Therefore, we conclude that the present work is compatible with the spin and parity assignment given in Ref. [15] and reported in Fig. 23, although more precise measurements are needed.

The lifetime analysis of all strong γ transitions of ^{50}Ca has been performed using the RDDS method on the Ca + Pb data. The $2^+ \rightarrow 0^+$ transition at 1027 keV was discussed in detail in Ref. [21]. From the relative intensity of the two components observed in the spectrum (corresponding to the decay before and after the degrader), the lifetime of the 2^+ state was measured to be $\tau = 96 \pm 3$ ps, which gives the reduced decay probability $B(E2) = 0.68 \pm 0.02$ Wu. This is in good agreement with shell-model calculations using isoscalar effective charges ($e_\pi = 1.5e$ and $e_\nu = 0.5e$), at variance from effective charge values previously obtained for fp shell nuclei around $N = Z$. As discussed in Ref. [21], this result suggests an orbital dependence of the effective charges in the fp shell.

All other transitions observed in the ^{50}Ca spectrum appear as fully shifted at each target-to-degrader distance. This is visible in the bottom panels of Figs. 24 and 25, where the γ spectrum of ^{50}Ca is shown after summing over all

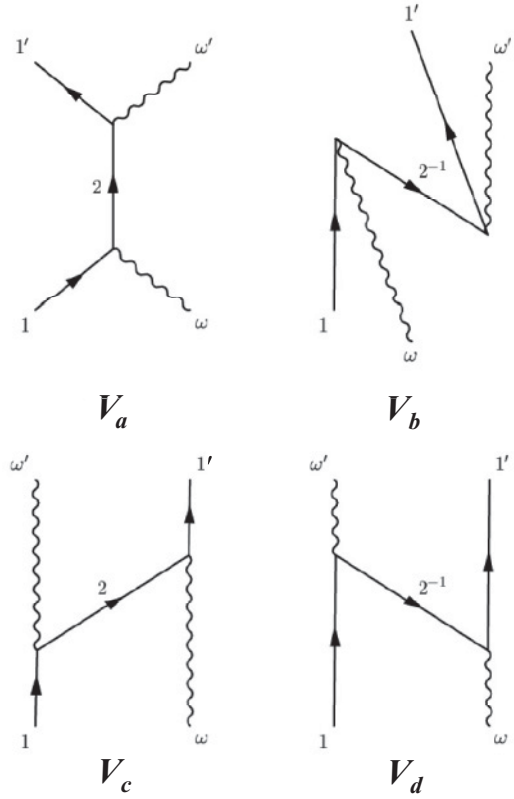

FIG. 26. Lowest-order diagrams contributing to the energy shift of a multiplet made up with a particle coupled to a vibration.

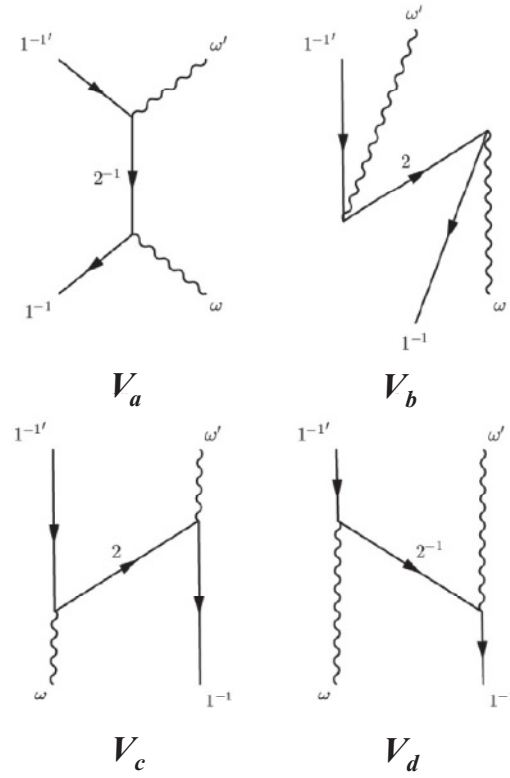

FIG. 27. The same as Fig. 26 in the case of a multiplet made up with a hole coupled to a vibration.

plunger distances. We note that at the expected energies of the transitions (marked by dotted lines) no peaks can be clearly observed, a part from the 3488-keV line, where traces of a second very weak component are seen, coming from the shortest measured distance of 30 μm [see inset of Fig. 25(c)]. This gives the upper limit $\tau < 1$ ps for the lifetimes of the 2^+, 3^-, 4^-, and 5^- states (assuming the typical value $v/c \approx 10\%$ and the shortest recoil distance of 30 μm). For the 4^+ state depopulated by the 3488 keV transition, a longer lifetime $\tau \approx 1.5$ ps is obtained from the intensity ratio of the two components observed at the 30-μm distance, although some delay may be given by the feeding of the short living transition of 595 keV. Therefore, we consider the 1.5-ps value as an upper lifetime limit for the 4^+ level (cf. Fig. 23). Table I summarizes the lifetime limits obtained for the ^{50}Ca states. We note that in the case of the $2^+ \rightarrow 2^+$ decay, the experimental $B(E2)$ value has been extracted from the lifetime of the second 2^+ state, taking into account the mixing ratio $\delta^2_{E2/M1} \approx 0.16$, as follows from the angular distribution analysis of the 1970-keV transitions. The overall analysis of the positive parity states of ^{50}Ca data shows that a rather global agreement with theory can be obtained using the full fp shell model previously employed in the case of the $2^+ \rightarrow 0^+$ decay (see discussion above).

VI. CONCLUSION

In this paper we have studied the γ decays of neutron-rich Ca isotopes around ^{48}Ca, populated by two heavy-ion transfer reactions, ^{48}Ca on ^{64}Ni, at 282 MeV, and ^{48}Ca on ^{208}Pb, at 310 MeV. The experiments were performed at LNL using the PRISMA-CLARA setup. The analysis shows the feasibility to perform full in-beam γ spectroscopy with heavy-ion transfer reactions in terms of angular distributions and polarizations, taking advantage of a large spin alignment, perpendicular to the reaction plane. This opens up the possibility to firmly establish, for the first time, spin and parity of excited states for a large number of n-rich nuclei which are hard to reach by standard fusion-evaporation reactions. The lifetimes of the excited states are also measured with the differential recoil distance method, applied to the ^{48}Ca on ^{208}Pb reaction, and the results are used to interpret the nature of the states.

We have discussed in particular the one-neutron transfer channels, ^{49}Ca and ^{47}Ca, where states arising by coupling a particle/hole to a phonon excitation of the doubly magic core ^{48}Ca are expected. The experimental data have been compared with predictions from full fp shell-model and PVC calculations. Evidence is found, in both nuclei, for particle/hole coupled states based on the 3^- phonon of the doubly magic ^{48}Ca core. This is the case of the $9/2^+$ state at 4.017 MeV in ^{49}Ca and of the $11/2^+$ state at 3.999 MeV in ^{47}Ca (the high-spin members of the particle/hole-phonon multiplets), which are favorably populated by the transfer reaction. Particular emphasis is given to the details of the particle/hole-phonon calculations, which are here revised and extended, as compared to the original model of Ref. [1]. This study gains insight into the robustness or softness of

core excitations and the interplay between single particle and collective degrees of freedom, which are at the basis of anharmonicities of vibrational spectra and at the origin of largely reduced spectroscopic factors. In the two-neutron transfer channels, ^{46}Ca and ^{50}Ca, the experimental data provide upper limits for the lifetimes of the majority of the observed states, in agreement with predictions based on shell-model calculations.

To conclude, the present work outlines an experimental method which can be exploited to further test nuclei in the vicinity of closed shell, setting up the stage for future systematic investigation with radioactive heavy-ion beams. In particular, moving away from the stability valley, this type of investigation will complement other, more direct, studies, such as single-nucleon transfer and knockout reactions [13,14]. This research will largely profit, in the near future, from the combined use of magnetic spectrometers and advanced γ arrays, such as the European project AGATA [67–69].

ACKNOWLEDGMENTS

This work was supported by the Italian Istituto Nazionale di Fisica Nucleare and partially by the Spanish MICINN (AIC10-D-000568 bilateral action and FPA2008-06419) and Generalitat Valenciana (Grant PROMETEO/2010/101). The work has also been partially supported by the Polish Ministry of Science and Higher Education (Grant No. N N202 309135).

APPENDIX: TECHNICALITIES OF PARTICLE/HOLE-PHONON MODEL CALCULATIONS

Within the PVC theory [1], at second order, there exist processes that generate an effective interaction between particle-phonon states and single-particle states. These processes lift the degeneracy of the particle-phonon multiplets. In the case of one particle outside the core these processes are discussed in detail in Ref. [1] (see p. 429 and Figs. 6–10). The four diagrams associated with energy shifts of the members of the multiplet are depicted here in Fig. 26 and have the following expressions (reported for the readers' convenience):

$$\langle j_1, n_\lambda = 1; IM|V_a + V_b|j_1, n_\lambda = 1; IM\rangle = \sum_{j_2} \frac{h^2(j_2, j_1, \lambda)}{\epsilon(j_1) - \epsilon(j_2) + \hbar\omega}\delta(j_2, I), \tag{A1}$$

$$\begin{aligned}\langle j_1, n_\lambda = 1; IM|V_c + V_d|j_1, n_\lambda = 1; IM\rangle &= \sum_{j_2} \frac{h^2(j_2, j_1, \lambda)}{\epsilon(j_2) - \epsilon(j_1) + \hbar\omega}\cdot\langle (j_2\lambda')j_1, \lambda; I|(j_2\lambda)j_1, \lambda'; I\rangle \\ &= \sum_{j_2} \frac{h^2(j_2, j_1, \lambda)}{\epsilon(j_2) - \epsilon(j_1) + \hbar\omega}\cdot(2j_1 + 1)\cdot \begin{Bmatrix} \lambda & j_1 & j_2 \\ \lambda & j_1 & I \end{Bmatrix}.\end{aligned} \tag{A2}$$

In the above equations j_i ($\epsilon(j_i)$) labels the single-particle states (and their energies), while λ ($\hbar\omega$) denotes the phonon state (and its energy). The coupling matrix element h has been already defined in Eq. (1). I is the angular momentum of the multiplet member.

In this work we are also interested in multiplets that are formed with a hole state coupled to a phonon. The same formalism applies and the corresponding diagrams are shown in Fig. 27 and have the following expressions:

$$\langle j_1, n_\lambda = 1; IM\,|V_a + V_b|\,j_1, n_\lambda = 1; IM\rangle = \sum_{j_2} \frac{h^2\,(j_2, j_1, \lambda)}{\epsilon\,(j_2) - \epsilon\,(j_1) + \hbar\omega}\delta\,(j_2, I)\,, \tag{A3}$$

$$\begin{aligned}\langle j_1, n_\lambda = 1; IM|V_c + V_d|j_1, n_\lambda = 1; IM\rangle &= \sum_{j_2} \frac{h^2(j_2, j_1, \lambda)}{\epsilon(j_2) - \epsilon(j_1) - \hbar\omega}\cdot\langle (j_2\lambda')j_1, \lambda; I|(j_2\lambda)j_1, \lambda'; I\rangle \\ &= \sum_{j_2} \frac{h^2(j_2, j_1, \lambda)}{\epsilon(j_2) - \epsilon(j_1) - \hbar\omega}\cdot(2j_1 + 1)\cdot \begin{Bmatrix} \lambda & j_1 & j_2 \\ \lambda & j_1 & I \end{Bmatrix}.\end{aligned} \tag{A4}$$

These latter equations can be obtained from the previous ones by means of particle-hole conjugation.

[1] A. Bohr and B. R. Mottelson, *Nuclear Structure*, Vols. I and II (W. A. Benjamin, New York, 1975).
[2] V. G. Soloviev, *The Theory of Atomic Nuclei: Quasiparticles and Phonons* (Institute of Physics Publishing, Bristol and Philadelphia, 1995).
[3] P. F. Bortignon, A. Bracco, and R. A. Broglia, *Giant Resonances: Nuclear Structure at Finite Temperature* (Harwood Academic, New York, 1998).
[4] M. B. Tsang *et al.*, Phys. Rev. Lett. **102**, 062501 (2009).
[5] G. Colò, H. Sagawa, and P. F. Bortignon, Phys. Rev. C **82**, 064307 (2010).
[6] E. Litvinova and P. Ring, Phys. Rev. C **73**, 044328 (2006); E. V. Litvinova and A. V. Afanasjev, *ibid.***84**, 014305 (2011).
[7] N. Pietralla *et al.*, Phys. Lett. B **681**, 134 (2009).
[8] P. Kleinheinz, Phys. Scr. **24**, 236 (1981).
[9] P. Kleinheinz, J. Styczen, M. Piiparinen, J. Blomqvist, and M. Kortelahti, Phys. Rev. Lett. **48**, 1457 (1982).
[10] S. Lunardi, P. Kleinheinz, M. Piiparinen, M. Ogawa, M. Lach, and J. Blomqvist, Phys. Rev. Lett. **53**, 1531 (1984).
[11] S. Gales, Ch. Stoyanov, and A. I. Vdovin, Phys. Rep. **166**, 125 (1988).
[12] C. J. Lister *et al.*, J. Phys. G: Nucl. Part. Phys. **6**, 619 (1980).
[13] K. L. Jones *et al.*, Nature (London) **465**, 454 (2010).
[14] A. Gade *et al.*, Phys. Rev. C **77**, 044306 (2008).
[15] R. Broda, J. Phys. G: Nucl. Part. Phys. **32**, R151 (2006).

[16] L. Corradi, G. Pollarolo, and S. Szilner, J. Phys. G **36**, 113101 (2009).
[17] A. Gadea *et al.*, Eur. Phys. J. A **20**, 193 (2004).
[18] D. Montanari *et al.*, Phys. Rev. C **84**, 054613 (2011).
[19] D. Montanari *et al.*, Phys. Lett. B **697**, 288 (2011).
[20] D. Mengoni *et al.*, Eur. Phys. J. A **42**, 387 (2009).
[21] J. J. Valiente-Dobon *et al.*, Phys. Rev. Lett. **102**, 242502 (2009).
[22] A. M. Stefanini *et al.*, Nucl. Phys. A **701**, 217c (2002).
[23] G. Montagnoli *et al.*, Nucl. Instrum. Methods Phys. Res., Sect. A **547**, 455 (2005).
[24] S. Beghini *et al.*, Nucl. Instrum. Methods Phys. Res., Sect. A **551**, 364 (2005).
[25] D. Montanari *et al.*, Eur. Phys. J. A **47**, 4 (2011).
[26] L. M. Garcia-Raffi *et al.*, Nucl. Instrum. Methods Phys. Res., Sect. A **391**, 461 (1997).
[27] D. Mengoni *et al.* Phys. Rev. C **82**, 024308 (2010).
[28] R. Broda *et al.*, Phys. Rev. C **82**, 034319 (2010).
[29] S. Szilner *et al.*, Phys. Rev. C **84**, 014325 (2011).
[30] P.-A. Soderstrom *et al.*, Phys. Rev. C **81**, 034310 (2010).
[31] H. Olliver, T. Glasmacher, and A. E. Stuchbery, Phys. Rev. C **68**, 044312 (2003).
[32] A. H. Wapstra *et al.*, *Nuclear Spectroscopy Tables*, Vol. VII (North-Holland, Amsterdam, 1959).
[33] T. Yamazaki, Nucl. Data A **3**, 1 (1967).
[34] T. C. Zhang *et al.*, Nucl. Phys. A **628**, 386 (1998).
[35] P. Aguer *et al.*, Phys. Rev. Lett. **43**, 1778 (1979).
[36] R. A. Eisenstein *et al.*, Phys. Rev. **188**, 1815 (1969).
[37] N. Benczer-Koller *et al.*, Phys. Rev. C **2**, 1037 (1970).
[38] T. Hartmann, J. Enders, P. Mohr, K. Vogt, S. Volz, and A. Zilges, Phys. Rev. C **65**, 034301 (2002).
[39] P. Federman and S. Pittel, Nucl. Phys. A **155**, 161 (1970).
[40] T. R. Canada *et al.*, Phys. Rev. C **4**, 471 (1971).
[41] E. Caurier, Shell-model code ANTOINE, IRES, Strasbourg, 1989.
[42] E. Caurier and F. Nowacki, Acta Phys. Pol. B **30**, 705 (1999).
[43] A. Poves *et al.*, Nucl. Phys. A **694**, 157 (2001).
[44] W. D. Metz, W. D. Callender, and C. K. Bockelman, Phys. Rev. C **12**, 827 (1975).
[45] R. Abegg, J. D. Hutton, and M. E. Williams-Norton, Nucl. Phys. A **303**, 121 (1978).
[46] Y. Uozumi *et al.*, Nucl. Phys. A **576**, 123 (1994).
[47] P. Martin *et al.*, Nuc. Phys. A **185**, 145 (1972), and references therein.
[48] M. E. Williams-Norton and R. Abegg, Nucl. Phys. A **291**, 429 (1977).
[49] S. Fortier *et al.*, Nuc. Phys. A **311**, 324 (1978).
[50] A. Winther, Nucl. Phys. A **594**, 203 (1995).
[51] A. R. Barnett *et al.*, Nucl. Phys. A **176**, 321 (1971).
[52] D. M. Brink, Phys. Lett. B **40**, 37 (1972).
[53] National Nuclear Data Center, Brookaven National Laboratory, http://www.nndc.bnl.gov/.
[54] B. A. Brown, Phys. Rev. C **58**, 220 (1998).
[55] E. Chabanat, P. Bonche, P. Haensel, J. Meyer, and R. Schaeffer, Nucl. Phys. A **643**, 441 (1998).
[56] L. Coraggio, A. Covello, A. Gargano, and N. Itaco, Phys. Rev. C **80**, 044311 (2009).
[57] D. E. Alburger, E. K. Warburton, and B. A. Brown, Phys. Rev. C **30**, 1005 (1984), and references therein.
[58] P. von Neumann-Cosel *et al.*, Phys. Rev. Lett. **82**, 1105 (1999).
[59] C. Lüttge *et al.*, Nucl. Phys. A **606**, 183 (1996).
[60] P. von Neumann-Cosel *et al.*, Phys. Lett. B **443**, 1 (1998).
[61] E. Caurier *et al.*, Phys. Lett. B **522**, 240 (2001).
[62] F. Nowacki and A. Poves, Phys. Rev. C **79**, 014310 (2009).
[63] G. Colò, P. F. Bortignon, S. Fracasso, and N. Van Giai, Nucl. Phys. A **788**, 173c (2007).
[64] G. Colò, L. Cao, N. Van Giai, and L. Capelli, Comp. Phys. Comm. (submitted).
[65] W. Kutschera *et al.*, Phys. Rev. C **12**, 813 (1975).
[66] K.-H. Speidel *et al.*, Phys. Rev. C **68**, 061302(R) (2003).
[67] D. Bazzacco, Nucl. Phys. A **746**, 248c (2004).
[68] A. Gadea *et al.*, Nucl. Instrum. Methods Phys. Res., Sect. A **654**, 88 (2011).
[69] S. Akkoyun *et al.*, Nucl. Instrum. Methods Phys. Res., Sect. A **668**, 26 (2012).